CHAPTER 4: The HRI Production Output

15 March 1984

On or about 1 JAN 1982, the "second pass" or "reprocessing" of all HRI observations was started. Based on the experience gained using EO data, the format of the production output was changed as were some of the data reduction routines. If you need a description of the original output, contact F. Seward, HEA/CFA.

The following is a list of abbreviations used:

ORP	Original Processing (as opposed to the "second pass")
PRD	Production run output
OCA	Observation Catalogue
PRF	Point Response Function
UM	User's Manual

The contents of Section 4 are:

4.0 Overview

4.1 Page 1 of PRD, the Title Page.

4.2 2 , the Processed Data Log.

4.3 3 , the Source Data Summary

4.4 4 , the Probability Output

4.5 5 Angular Size Data

4.6 6 Variability Output

4.7 Contour Diagram, Mini Catalogues

4.8 The Log of the processing

4.9 Aspect Plots

4.10 Conversion of Count Rate to Flux

4.11 Integrity of the Image

4.0 Overview

The E.O. data stream is broken up into time segments of variable length. These are called "HUTS" (HEAO Universal Time) and are designated by their initial major frame number (±1). Major frames are time units equal to 40.96 seconds.

A particular observation normally will contain more than one HUT, but the first phase of the production run (PRD) operates on individual HUTS to obtain the Aspect. The sequence of programs run is shown below followed by a brief description of each element and a list of files produced. The MERGE processing puts the individual HUTS together and operates on the whole data set.

Once the image is "constructed", the background is measured, the statistics are assembled to decide the DETECT threshold which should, on average, yield one false source per field. DETECT and CENTROID find and define discrete sources. The methods of obtaining source parameters will be described in the following sections.

INPUT PHASE	PRDSYM			
	MINICAT			
	ADDBASE			
	PUPDATE			
	HSKPNG			
	PUPDATE			
	PCGDURA			
	EDBM		CALCULATING	
HUT	ASPECT1	–	ASPECT	(A)
PROCESSING –	NEWBORE		SOLUTION	
	ADDBASE			
	QLPLT			
	ASPECT2			
	ASPECT3			
	ASPECT4			
	COMPRESS			
	SS PLOT			
	RDFID			
	HPROD	–	MAKING IMAGE	(B)
	HSORT			
	MERGETGR			
	HIMAGE			
	TIPI			
	QLPLT			
	BKGRD			
	DETECT			
MERGE	CONTIG			
PROCESSING –	DETECT1	–	SOURCE DETECTION	(C)
	CONTIG1			
	CENTROID			
	HGAIN			
	HEXPOSURE			
	FTCOR	–	SOURCE ANALYSIS	(D)
	BIVARY			
	HFLUX			
	HEAOMAP			
	GZCONT			
	HEAOMAP	–	OUTPUT	(E)
	HRIPRINT			

HUT PROCESSING

INPUT PHASE

PRDSYM — Creates Processing Directory with .PCG file, .Info File, Symbol Table and Links to .PRD Files.

HUT PROCESSING

MINICAT — Gathers star catalogue info. Creates .SCAT and .CAT Files.

ADDBASE — Extracts raw FIDCAL Info from Database.

PUPDATE — Updates .PCG File with FIDCAL on/off times.

HSKPNG — Uses .ACD file to update PCG File with
a) Status of:
(i) Voltage (on/off)
(ii) Filters
(iii) SAAD
(iv) Grating
(v) BOD
b) Creates .QPI File with BOD SAAD and Filter Values to be Plotted.

PUPDATE — Updates PCG File with Results of Housekeeping Run.

PCGDURA — Calculates Instrument Calibration Durations.

EDBH — Creates .MAG File containing Earth Blocking and magnetic field information from Ephembase.

ASPECT1 — Checks Aspect Data for each minor frame for validity. Applied calibration correction to tracker and gyro data.

NEWBORE — Creates .BSD file containing processed FIDCAL values.

ADDBASE — Writes processed FIDCAL values into Database.

QLPLT — Creates plot of Aspect solution.

ASPECT2 — Produces aspect solution for intervals when star trackers were locked on two guide stars; folds with gyro data.

ASPECT3 (MAPMODE) — Used to augment ASPECT2 when star trackers not locked on guide stars; identifies other stars tracked.

ASPECT4 — Uses stars identified by ASPECT3 to produce result similar to ASPECT2.

COMPRESS — Extracts extraneous data from HRI-.PRD file. Remaining data is compressed. Can also delete data occurring during Earth occultation, whether indicated by .MAG or .PCG files. OUTPUTS: .BKB, .SS, .COM, .MFT.

SSPLOT	Adds secondary science information from .SS file to .QPI file.

MERGE PROCESSING

RDFID	Extracts FIDCAL information from database, to be used by HPROD to correct pointing direction.
HPROD	Refines .COM files. Applies Aspect and GAPMAP correction and Hotspot masking. Outputs: puts primary science into .QPI .XPR, .HDR, .MPT, .TGR.
HSORT	Reads XPR and .HDR Files to create a single .SRT file.
MERGETGR	Merges TGR files for later use in timing analysis.
HIMAGE	Creates image file from .SRT File.
TIPI	Calculates time in processed image.
QLPLT	Creates Science Strip Plots from QPI Files.
BKGRD	Computes average background for 12x12 arcsec bin, determines thresholds for six detect cell sizes and stores values in SDF File.
DETECT	Slides detect window over image, marking for future processing by CONTIG those areas with a count above given threshold. Window sizes 12x12, 24x4, 36x36 used.
CONTIG	Calculates centers of all contiguous source locations. Outputs list of sources in .SDF.
DETECT1	Same action as DETECT except that window sizes 48x48, 72x72, and 120x120 are used and the search area is confined to a circle of radius = 5 arcmin, centered at the field center.
CONTIG1	Similar action to CONTIG.
CENTROID	Determines center of each source found by DETECT and CONTIG. Determines uncertainty of centroid.
HGAIN	Calculates instrument gain.
HEXPOSURE	Reads .MPT Files to create two exposure files. One with quantum efficiency (.QEX) and one without (.BEX).
FTCOR	Calculates barycentric time corrections from Ephemeris base.
BIVARY	Performs source variability studies. If not enough photons for a source are found, then flare analysis performed. Outputs

one .ISF file per source.

HFLUX — No longer calculates flux. Applies corrections to source counts to obtain (Net/1000).

HEAOMAP — Makes plot of known star positions (.MCPL).

GZCONT
HEAOMAP — Makes contour plot of detected sources (.SCONT).

HRIPRINT — Formats print output.

DESCRIPTION OF CONTENTS

INPUT FILES

ASP -	.PRD	Raw Aspect Data.
HRI -	.PRD	Raw Science Data.

OUTPUT FILES

FILE		
ASP -	.PRN	Aspect Solution (text).
ASP -	.PRD	Aspect Solution -
	.CAT	Part of Master Star Catalogue that lies in HRI field of view.
	.SCAT	Star Catalogue Information relating to tracker fields.
	.PLST	PCG Information List.
	.QPI	Plotting Information.
ASP -	.QPLT	Aspect Strip Plot.
	.COM	Compressed Photons.
	.SS	Secondary Science Data.
	.BKB	Data for Future High Background Analysis.
	.MFT	Major Frame Timing File.
MERGE		
	.MLST	List of Merging Huts.
	.XPR	Further screened compressed photon information, with

		GAPMAP and aspect correction applied.
	.HDR	Information relating to .XPR file.
	.MPT	Aspect correction (exposure) maplet.
	.TGR	Timing gap records.
	.IMG	Image.
	.SRT	Sorted Photons.
	.BPF	Boresite Parameters.
	.HLST	Star Catalogue Information (text).
	.MCPL	Catalogued Star Plot.
	.SCONT	Contour Plot of Detected Sources.
	.SDF	All Source Information, Locations, Counts, etc.
	.ISF	List of source photons extracted from true .SRT file (with timing correction applied).
HRI -	.QPLT	Science Strip Plot.
	.QEX	Exposure File (with quantum efficiency).
	.BEX	Exposure File (without quantum efficiency).
	.UPD	OCA Update Information.
	.OUTPUT	Text File of Program Outputs.

4.1 The Title Page

The aim of the revised format was to make the HRI production print-out as self-contained and self-explanatory as possible; therefore, not every item of the output will be discussed here.

Interspersed with this running commentary will be annotated examples of an HRI production run, labeled as List 4.1, etc.

Small differences between the "target position" and the "field center" may arise from inaccuracies in the OCA

"DOP" means the "detailed observing program" (produced by Goddard just before the commands were sent to the satellite). The "Net time in the processed image" is the total number of seconds during which incident photons could be recorded.

```
**********************************************************************
*      CFA EINSTEIN HRI Production Processing System.  Field Data Summary.   *   THURSDAY  20-JAN-83  03:17:55     Page  1
**********************************************************************
```

Observation Title: 4U 1700-37 (HD 153919), GALACTIC SOURCE LOCATION AND SPECTRA

Sequence Number: 1043
Observer ID: 0 (0 = CFA, 1 = Columbia, 2 = M.I.T., 3 = Goddard, 4+ = Guest)

Target RA, DEC (from DOP): 17h 0m 32.60s -37d 46' 29.9" (Nominal RA, DEC) } 1950 Coordinates

Field Center (1950) RA, DEC: 17h 0m 32.62s -37d 46' 28.5" (Binned RA, DEC) }

255.13590 -37.7746 degrees

Y=2047.5 Z=2047.5 pixels

L= 347.7542 B= 2.1741 <---------- Galactic Coordinates

Net time in processed image: 1199.7 secs.

Start time of 1979 day 78 (19-MAR-79) at UT 0H 47M 25.7S and
End time of 1979 day 78 (19-MAR-79) at UT 1H 26M 20.4S.

Number of photons within 9 arcmins radius of center of image: 1424.

Nominal roll angle from DOP: -98.66 degrees
Binned roll angle : .00 degrees
(With normal complete processing (North as -Z), the binned roll angle should be zero.)

Dead time correction for this observation is: 1.02

The gain for the source with the most counts in a 12"x12" detection cell should be 7. +/- 2.5.
For this observation, the value is: 5.97 <---------- If outside the specified range, contact P. Henry, U. of Hawaii.

The HRI sub-instrument used was number: 3

The global background level is .000281 +/- .000007 cts/pixel/1000 secs. (From the whole field)
For DETECT, background is .000337 +/- .000013 cts/pixel/1000 secs. (From circle of radius 5.0 arcmins)

For the standard circle of radius = 18", background is 1.6463 cts

For detection cell of	12"x12"	24"x24"	36"x36"	48"x48"	72"x72"	120"x120"
Background is	.2329	.9316	2.0962	3.7266	8.3848	23.2910
Source threshold is	4.8626	6.5879	10.0384	13.6263	20.2142	43.3294

Standard information .....

1 pixel = 0.5 arcsec x 0.5 arcsec
Tangent plane geometry is assumed.

The "Nominal Roll Angle" is a clockwise rotation about the space craft's X-axis (aiming at the target on the celestial sphere). It relates the focal plane instrument's orientation with respect to RA and DEC.

The DEAD TIME CORRECTION measures the fractional time during which the detector is unable to record events because it is "processing" a prior event. (DTC is a function of the total field count rate.)

The DETECT background is calculated over a smaller area than the GLOBAL BACKGROUND in order to avoid edges of the HRI image which, late in the mission, exhibited splotchy areas of higher count rate. The DETECT BACKGROUND is the value used in all calculations.

****

NB After the end of processing, a major flaw was found in the algorithm used for background determination. This flaw usually produced an erroneously high DETECT background whenever a strong source was within 5' of the field center. The impact for such fields is three-fold: (a) weak sources will fail the threshold for DETECT and thus be ignored, (b) source intensities will be incorrect because too large a value of BG was adopted, and (c) the estimate of intensity for weak, extended sources will be underestimated. To understand the problem, we digress to a description of the background algorithm.

First, the 4096 array in which the HRI image is imbedded (center at 2047.5, 2047.5) is zoomed by 256; i.e. 256^2 pixels are summed and each sum becomes one element of a 16x16 array.

For the global background the average background level and 3σ deviation is found for all array elements within 9' from the field center (50 some elements). Next, all elements which are greater or less than 3σ from the average are rejected and a new average is found; "the global background."

For the reasons given above, the DETECT background initially considers only elements within 5' (some 16 elements) of the field center. What occurs now in the presence of a strong source is that the average of 16 elements is raised significantly so that some, most, or all of the normal (unaffected by the presence of a source) elements are rejected because they fall below the (Average - 3σ)! Obviously, the remaining elements are usually contaminated by source counts, and a large DETECT background results. Future processing should be made to eliminate the "3σ below" rejection.

Figure 4.1 is a plot of DETECT and GLOBAL backgrounds as a function of (NET/1000). The effect of the flaw on the global background is mitigated by the larger number of elements averaged. You may judge the importance of the flaw for any particular field and decide if a correction to the background is necessary for your source intensities.

For the present, the only method of recovering weak sources is to repeat (off-line) Sections C, D, and E of the processing (see Section 4.0).

****

4.2 Page 2: The Processed Data Log.

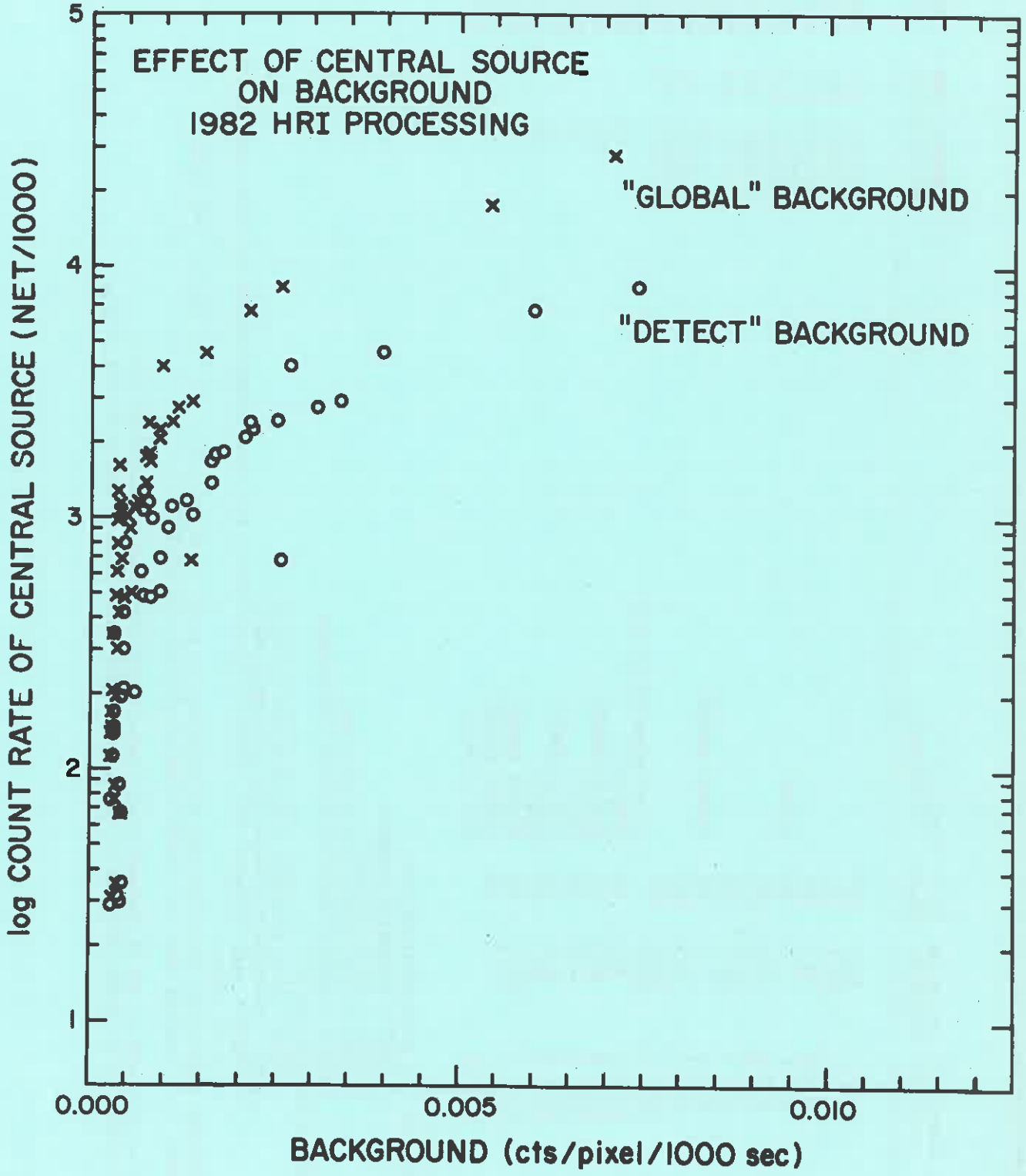
EFFECT OF CENTRAL SOURCE
ON BACKGROUND
1982 HRI PROCESSING
"GLOBAL" BACKGROUND
"DETECT" BACKGROUND
log COUNT RATE OF CENTRAL SOURCE (NET/1000)
BACKGROUND (cts/pixel/1000 sec)
5
4
3
2
1
0.000
0.005
0.010

Figure 4.1

Interval Number	Starts at (seconds)	Duration (seconds)	Data used?	Reason deleted.....	Aspect solution	Sep. Err.	Major frame	Minor frame
1	27.8	54.1	YES		MAPMODE	2-4	0266221	77
2	81.9	286.7	YES		LOCKED	2-4	0266222	118
3	368.6	78.1	YES		MAPMODE	2-4	0266229	110
4	446.7	.6	NO	TLMDRP	MAPMODE	2-4	0266231	106
5	447.4	85.1	YES		MAPMODE	2-4	0266231	108
6	532.5	41.0	YES		MAPMODE	4-6	0266233	110
7	573.4	398.1	YES		LOCKED	4-6	0266234	118
8	971.5	.6	NO	TLMDRP ASPECT	NO		0266244	82
9	972.2	51.8	YES		LOCKED	4-6	0266244	84
10	1024.0	204.8	YES		MAPMODE	4-6	0266245	110
	1228.8	923.5		Inter-observation gap			0266250	118
11	2152.3	8.3	NO	ASPECT	NO		0266273	60
12	2160.6	20.5	NO	HIBKGD ASPECT	NO		0266273	86
13	2181.1	10.2	NO	ASPECT	NO		0266274	22
14	2191.4	10.2	NO	HIBKGD ASPECT	NO		0266274	54
15	2201.6	10.2	NO	ASPECT	NO		0266274	86
16	2211.8	122.9	NO	HIBKGD ASPECT	NO		0266274	118
17	2334.7	3.2	NO	EARBLK ASPECT	NO		0266277	118
	2337.9			End of data			0266278	0

Notes to the log:

Reasons for data deletion are:

- TLMDRP = telemetry dropout
- EARBLK = earth blocked
- HIBKGD = high background count rate
- ASPECT = aspect solution was not acceptable

Aspect categories are:

- LOCKED = star trackers locked on guide stars
- GYRO = extrapolated solution using gyro data
- MAPMODE = star trackers not locked on guide stars, but stars observed and solution calculated
- NO = no aspect

Average separation error between guide stars is given in arcseconds. In the case of map mode, this is an average over all stars observed during the segment.

A major frame is 40.96 seconds long, and a minor frame is 0.32 seconds long.
Time 0.0 is at minor frame 0 of the first major frame of this observation.

L4.2

This page is also self-explanatory. The log is useful for evaluating the aspect quality of your data, deciding if "lost" data might be recovered (together with the Aspect plots; 4.9), and how to choose data segments for special purposes.

4.3 The Source Data Summary (Page 3)

Our intention has been to collect the most useful data about each source on this page.

Source Selection

The basic method of source detection is a bit map in which flags are set "on" whenever the sliding "DETECT CELL" finds a value of counts greater than a set threshold. ALL contiguous or overlapping "ON" cells are coalesced by CONTIG which also finds an "average" center. CENTROID finds the source position as the centroid of all counts within a DETECT CELL placed on the average center.

The whole field is subjected to DETECT cells of 12", 24", and 36". The larger cells (48", 72" and 120") are accepted only if they occur within 5 arcmin of the field center.

Astrometric Quality of HRI Positions

The HRI was designed to allow positions of X-ray sources to be determined to arcsec accuracy providing enough counts were detected for reliable centroiding of HRI data. As most users of the HRI data know, a number of systematic effects (magnetic distortions, position of the HRI in the focal plane) were identified in the early data processing and correction procedures were developed. The magnetic distortion effects were removed to first order in HRI processing after February 1, 1980, and in final form after April 1, 1980. The position of the HRI in the focal plane was corrected (by interpolation over the FIDLITE data base) in a complete way only in the final reprocessing of the HRI data.

The astrometric quality of the HRI positions is thus dependent on the date of processing. The positional accuracy achieved was determined (for each processing epoch) by comparing the detected vs. true (optical or VLA) positions for a number (~10-20) of identified sources. These sources were in general different from those (~10) used to derive the so-called "boresite parameters" which give the alignment of the X-ray vs. optical (star tracker) axes of the Einstein Observatory. The distribution of detected vs. true positions was evaluated (for each epoch of processing) and found to be well-described by a two-dimensional Gaussian, as expected. The 90% confidence radii (i.e., radius in which 90% of the known sources were detected) was then determined. The results are:

HRI Processing Period	90% Confidence Radius
Before February 1980	~10 arcsec
February 1 - April 1, 1980	~5 arcsec
April 1, 1980 - December 1981	~4 arcsec

January - June 1982 (First HRI reprocessing)	~3.5 arcsec
July 1982 (Final HRI reprocessing)	3.2 arcsec

The approximate nature of the position accuracies prior to final reprocessing is due to several effects - primarily the dependence of the actual HRI detector used (i.e., date of observation). The final HRI reprocessing makes use of the boresite parameters which were determined separately for the three major epochs of Einstein HRI data: from launch through January 1979 (HRI-2), from January 1979 - August 1980, when the Observatory operations were interrupted, and from December 1980 - April 1981, when observations resumed until the end of the mission. Positional accuracies finally achieved appear to be comparable for the last two periods, although a figure of 4.9 arcsec is more appropriate for HRI-2 (November and December 1978).

For any of the 90% confidence radii given above, the corresponding 1σ values can be obtained by dividing by 2.15 (since 90% confidence radii are at 2.15σ for a 2-D Gaussian). The 1σ radii are useful if N <u>independent</u> (i.e., using different guide stars or, at least, a different source position on the detector) observations of the same source are to be combined. This will yield a more accurate source position, since the positional uncertainty can then be reduced by a factor $\sim N^{1/2}$. A full discussion of the Einstein HRI positional accuracies achieved is given by Grindlay et al (1984, <u>Ap.J.</u> (Letters) submitted)) in their discussion of the analysis of precise positions of bright globular cluster X-ray sources. It was this project which motivated the entire analysis of HRI position accuracy.

The statistical errors associated with each source are listed in the Source Data Summary table and should be added in quadrature to the systematic uncertainties discussed here.

<u>Estimates of Source Intensity</u>

"BCTS" (box counts) and CCTS (circle counts) are reconstructed (after DETECT finished) by placing the appropriate box or circle on the source position. These numbers are not used in any way; they are printed here to help you evaluate the quality of the detection. Because of the quantum steps in the "sliding" of the DETECT BOX, and the subsequent determination of the centroid, BCTS and CCTS may be less than threshold.

The fundamental measurement and appropriate corrections are based on the "standard circle" (radius = 18 arcsecs).

Instead of trying to measure the size of extended sources (assuming they were circularly symmetric) and then correcting the intensity, we have constructed a circle which encompasses all of the contiguous detection cells, and calculated the corresponding "NET/1000" for this "extended circle." SIZCOR = (NET/1000) EXT CIR/(NET/1000) STD CIR. It provides a first approximation to use for count rates and flux of extended sources.

* CFA EINSTEIN HRI Production Processing System. Source Data Summary. *

SOURCE *	RA HMS / DEGS / PIX	+/-	DEC DMS / DEGS / PIX	+/-	DETECT BCTS / CCTS	CORS DEC / VIGN / EPT	STD CIR CTS / SCSC / NET/1000	+/-*	CONTIG CELL CIR YCC / ZCC / REC	ECSC / SIZCOR	VARY SIZE PUR
Sources found in pass of 12"x 12" detection cell, stepped at 4" intervals with threshold 4.9:											
1	17h 0m 32.70s	.04s	-37d 46' 28.3"	.50"	143.0	1.04	198.0	14.1	2045.1	1.18	NEGATIVE
	255.13620d	.0001d	-37.77452d	.0001d	147.0	1.00	1.26		2044.5	1.0	.145
	2045.7p	1.0p	2047.0p	1.0p		1199.7	218.0	15.7	29.7		

* W A R N I N G *

The following list of sources found with DETECT BOXES larger than 12"x 12" may include more than one spurious source per field.

Sources found in pass of 24"x 24" detection cell, stepped at 8" intervals with threshold 6.6:											
2	17h 0m 34.21s	1.0s	-37d 46' 22.1"	12.00"	15.0	1.04	77.0	8.8	1991.5	1.18	NEGATIVE
	255.14250d	.0033d	-37.77281d	.0033d	21.0	1.01	1.26		2031.5	2.5	.000
	2009.9p	24.0p	2034.7p	24.0p		1199.7	84.0	9.9	29.5		
3	17h 0m 31.04s	.51s	-37d 46' 6.1"	6.00"	9.0	1.07	10.0	3.2	2087.5	1.25	NEGATIVE
	255.12930d	.0017d	-37.76836d	.0017d	9.0	1.01	1.26		2007.5	1.2	.011
	2085.2p	12.0p	2002.7p	12.0p		1199.7	9.0	3.7	19.8		
4	17h 0m 31.66s	.55s	-37d 47' 2.1"	6.50"	6.0	1.01	7.0	2.6	2079.5	1.22	NEGATIVE
	255.13190d	.0018d	-37.78391d	.0018d	7.0	1.01	1.27		2119.5	1.5	.124
	2070.2p	13.0p	2114.6p	13.0p		1199.7	5.0	2.9	22.8		
Sources found in pass of 36"x 36" detection cell, stepped at 12" intervals with threshold 10.0:											
5	17h 0m 32.88s	.34s	-37d 45' 40.3"	4.00"	10.0	1.10	9.0	3.0	2051.5	1.17	--------
	255.13700d	.0011d	-37.76118d	.0011d	9.0	1.01	1.27		1955.5	2.0	.151
	2041.0p	8.0p	1951.0p	8.0p		1199.7	8.0	3.6	31.1		

NOTES TO THE TABLE

POSITIONS: Centroid of all counts within detection cell centered on source position. The +/- values define the 90% error box.

For the standard detection cell:

BCTS: The observed counts in the standard size DETECT box (12", 24", 36", 48", 72" or 120"), centered on the source.
CCTS: The observed counts in the corresponding circle (diameter = 13.54", 27.08", 40.62", 54.16", 81.24" or 135.4").

Corrections:

QEC: The quantum efficiency correction which is a function of Y,Z.
VIGN: The vignetting correction for 1 keV.
EPT: The exposure time given in seconds.

For the standard circle with radius = 18", centered on the source centroid:

CTS: The observed counts in the circle.
SCSC: The standard circle scattering correction. This approximately corrects for the source counts which fall outside the standard circle. It is derived from the 1 keV point response function and depends on the distance from the field center.
NET/1000: The approximate count rate per 1000 secs, equal to (CTS-BG) * DTC * VIGN * QEC * SCSC * (1000/EPT), where DTC is the dead time correction and BG is the background counts in an 18" radius circle.

For the circle which encompasses all contiguous detect cells:

Ycc and Zcc: The pixel coordinates of the center of the circle.
REC: The radius of the "extended" circle in arcsecs. If REC is less than or equal to 18", ECSC and SIZCOR are not calculated, and are set to -1.0.
ECSC: The extended circle scattering correction.

N.B.: ECSC will generally be too small for truly extended sources. If the actual source distribution were known, a more accurate value of ECSC could be obtained ex post facto.

SIZCOR: The size correction to be used for estimating the count rate, flux, etc. of extended sources:

(NET/1000) OF CONTIG CELL CIR. = SIZCOR * (NET/1000) OF STD. CIR.

NB: The background subtraction used in the derivation of SIZCOR could be too large if part of the extended circle falls outside of the (masked) HRI field.

SIZE PUR: The probability that the source is unresolved. A parameter is calculated which is a measure of the difference between the source's radial distribution (see page 5) and that expected from a point source at the same distance from the field center. PUR is the probability of obtaining this value of the parameter by chance from an unresolved source. The algorithm is not accurate for "uninteresting" values

Because of the "flaw" described at the end of Section 4.1, the presence of a strong source may have a significant effect on SIZCOR of weak, extended sources. First, REC, the radius of the extended circle which encompasses all contiguous DETECT cells may not be as large as it should have been, and thus the outer edges of faint sources may be missed. Second, because the integration circle is usually much greater than the standard circle, the background subtraction becomes more critical, and the over-estimated background level will reduce the total source counts by a larger factor than for the standard circle.

In the example for H1043 (List 4.3) source #1 is the strong (target) source. Although there were many DETECT cells above threshold (radius of extended circle = 30 arcsec), NET/1000 (extended circle) = NET/1000 (std. circle) since the source is unresolved and SIZCOR = 1.0 as it should be.

Sources 2, 3 and 4, found with the 24" cell probably represent statistical fluctuations in the wings of #1. The extended circle calculation for #2 appears to have recovered most of the counts in #1: SIZCOR = 2.5 and NET/1000 (extended circle) = 2.5*84 = 210 (c.f. 218. for #1).

Other Parameters

SIZE PUR (probability unresolved) and VARY are described in the notes to the table. These indicators have never been subjected to a critical evaluation. Therefore, if a positive result is flagged, a careful analysis should be performed off line, from the radial output (Section 5), or from VARIABILITY output (Section 6).

4.4 The Probability Output, Page 4

Statistical data from the 12" DETECT are saved and printed out on this page (the "Histogram"). If there were no real sources in the field and given the average background (page 1), then the number of occurrences of finding n counts in a cell from Poisson statistics is given in the column "# Expected Sources".

4.5 Angular Size Data, Page 5

To assist the user in evaluating the radial distribution for a particular source, the PRFs for 4 energies and 2 positions are listed. For source #1, half of the counts within the standard circle are contained in a circle with r = 4.0 arcsec. This agrees with the PRF for 2.98 keV, R = 0 (3.96 arcsec). The other sources have pathological distributions since they are positioned on the flanks cf #1.

An analytical approximation to the 1.5 keV PRF for the field center has been constructed by P. Henry:

$$PSF(r) = 2.885 \times 10^{-2} \quad \exp(-r/1\farcs96) + 0.01 \exp(-r/12\farcs94) \quad \text{arcsec}^{-2}$$

This was derived from some long exposures of point sources on axis. It appears to be a reasonably accurate description within 5' of the field center for sources such as Cxg X-2 and 3C272 (i.e. non-pathalogical spectral

CTS(12")	PROB RANDOM	* EXPECTED SOURCES	* OBSERVED SOURCES	PROB ALL RANDOM
3	.177E-02	87.08	1	.100E 01
4	.102E-03	7.25	1	.999E 00
5	.471E-05	.33	1	.283E 00
6	.182E-06	.01	1	.120E-01
7	.602E-08	.00	1	.425E-03
8	.175E-09	.00	1	.123E-04
9	.451E-11	.00	1	.318E-06
10	.105E-12	.00	1	.743E-08

PROB RANDOM is the probability that any particular 12 arcsec box has this many counts (at random).

* EXPECTED SOURCES is the number of 12" arcs expected to have this many counts (from the statistics).

* OBSERVED SOURCES is the total number of sources with an observed intensity greater than or equal to CTS in the 12" box.

14.4

****** HISTOGRAM OF # OF PHOTONS(1-46) PER 12X12 SEC BIN ******

1 CT/BN	2 CT/BN	3 CT/BN	4 CT/BN	5 CT/BN	6 CT/BN	7 CT/BN	8 CT/BN	9 CT/BN	10CT/BN	11CT/BN	12CT/BN	13CT/BN	14CT/BN	15CT/BN	16CT/BN
20380	2027	185	26	7	5	2	1	0	0	2	1	0	1	1	1

17CT/BN	18CT/BN	19CT/BN	20CT/BN	21CT/BN	22CT/BN	23CT/BN	24CT/BN	25CT/BN	26CT/BN	27CT/BN	28CT/BN	29CT/BN	30CT/BN	31CT/BN	32CT/BN
1	2	0	2	1	0	2	0	0	0	0	1	0	0	0	0

33CT/BN	34CT/BN	35CT/BN	36CT/BN	37CT/BN	38CT/BN	39CT/BN	40CT/BN	41CT/BN	42CT/BN	43CT/BN	44CT/BN	45CT/BN	46CT/BN
1	0	0	0	0	0	0	0	0	0	1	0	0	1

The Huntsville Calibration Data describe the point response function. In addition to the radii of the annular bins, the fraction of all source counts which fall outside of the standard 18" circle is given in the last column.

Huntsville Calibration Data: Outer Radii (arcsecs)

	ENERGY (keV)	DISTANCE FROM FIELD CENTER (arcmins)	BINS 1	2	3	4	5	6	7	8	9	10	FRACTION BEYOND 18"
A	.277	0	1.08	1.65	2.19	2.75	3.41	4.22	5.27	6.72	9.40	18.00	0.17
B	1.49	0	1.13	1.77	2.40	3.10	3.89	4.83	5.98	7.65	10.56	18.00	0.25
C	2.98	0	1.12	1.75	2.38	3.12	3.96	4.91	6.17	7.93	11.15	18.00	0.40
D	4.51	0	1.49	2.32	3.17	4.10	5.27	6.50	7.97	9.85	12.92	18.00	0.51
E	.277	10	2.52	4.50	6.17	7.65	9.08	10.53	12.06	13.74	15.65	18.00	0.24
F	1.49	10	2.35	4.02	5.78	7.31	8.74	10.21	11.81	13.56	15.68	18.00	0.37
G	2.98	10	2.42	4.32	6.12	7.70	9.29	10.79	12.36	13.96	16.33	18.00	0.52
H	4.51	10	2.81	4.71	6.29	7.86	9.41	10.82	12.41	14.17	16.15	18.00	0.65

14.5/1

467

RADIAL OUTPUT FOR THIS OBSERVATION

SOURCE	1	2	3	4	5	6	7	8	9	10	TOTAL 18	
1	20.0	25.0	15.0	21.0	18.0	20.9	18.3	19.9	19.7	18.0	196.4	CTS PER RING
	1.20	2.10	2.50	3.10	4.00	5.10	6.20	7.40	11.10	17.80		OUTER RADII (SEC)
	4.44	2.56	3.00	1.79	.95	.65	.49	.30	.09	.03		PHOTON DEN/ARCSEC2
2	7.6	7.6	8.8	6.9	7.8	6.9	7.5	8.0	7.9	6.9	75.4	CTS PER RING
	8.60	12.50	14.10	14.70	16.00	16.40	16.60	16.80	17.50	18.00		OUTER RADII (SEC)
	.03	.03	.07	.13	.06	.13	.32	.36	.11	.12		PHOTON DEN/ARCSEC2
3	1.0	1.0	.8	.8	1.0	.9	.9	1.0	.9	.4	8.6	CTS PER RING
	1.00	2.80	6.40	8.40	8.60	9.60	10.70	11.10	12.20	16.50		OUTER RADII (SEC)
	.31	.05	.01	.01	.09	.02	.01	.04	.01	.00		PHOTON DEN/ARCSEC2
4	1.0	1.0	.9	-.0	.8	.9	-.0	1.0	.6	-.0	6.1	CTS PER RING
	.40	2.50	5.50	5.60	8.20	9.80	9.90	10.00	13.50	13.60		OUTER RADII (SEC)
	2.00	.05	.01	-.00	.01	.01	-.00	.17	.00	-.00		PHOTON DEN/ARCSEC2
5	1.0	.9	.9	.4	.9	.9	.9	.7	.9	-.0	7.5	CTS PER RING
	.50	4.00	5.70	12.40	13.50	13.50	14.70	16.60	17.20	17.30		OUTER RADII (SEC)
	1.33	.02	.02	.00	.01	.03	.01	.00	.01	-.00		PHOTON DEN/ARCSEC2

795

The maximum radius is 18 arcsecs.
The 10 radial bins are chosen so that 10% of the counts within the 18" circle appear in each bin.
The CTS PER RING and PHOTON DENs have been corrected for background.

14.5/2

distributions) as well as for 1.5 keV ground calibration data. It is good for r out to about 1 arcmin.

Three instrumental effects which may distort the circular symmetry of an unresolved source are discussed in section 4.11.

4.6 Variability Output, Page 6

Two analyses are performed to measure deviations from steady emission. Photon arrival times are used to search for low frequency (non-periodic) fluctuations and intervals between arrivals are used for high frequency fluctuations. The Smirnov-Cramer-von Mises test is used for small numbers of photons (statistic="NW**2"), and the chi-squared test (statistic="chi-squared"; degrees of freedom = "DOF") is used for larger numbers. The column headed "PROB" gives the probability of obtaining that value of the statistic from a steady source. For reasons that are unclear to the present writer, probabilities based on intervals (the second line of each entry) are usually much smaller (sometimes by 4 orders of magnitude) than probabilities based on arrival times for processing which occurred early in 1982. However, for processing in September and October 1982, the situation seems to be the reverse. Until an exhaustive evaluation of the secular probabilities is carried out, these indicators should be used with extreme caution.

For the Fourier analysis, the column headed "FOUR COEFF" gives the largest value of the Fourier amplitude for all of the frequency bins tested. The column "PROB" gives the probability that a steady source would yield the given value of "FOUR COEFF", and the column headed "PERIOD" gives the associated period in seconds. Since the Fourier coefficient has been normalized by the exposure time and the (# of photons)$^{1/2}$, there is a 1-1 correspondence between the coefficient and the probability. The probability falls to 10% at a coefficient of 3.28 and to 1% at 3.44.

4.7 The Contour Diagram

The image is displayed by contouring an array constructed with a compression factor ("ZOOM") of (32 pixels/element)^2. Unfortunately, this leads to a poor representation of weak features, which may be distorted, depending on how the array center is chosen.

A plot showing the positions of objects from the mini catalogues is also given, and the catalogued objects are listed.

4.8 The Log of the Processing

This log is useful for evaluating problems. Since most of the information is given in a rather cryptic way, we will not attempt to describe it here.

4.9 The Aspect Plots

The strip charts at the end of the PRD output come in 2 sets. Within each set there is one plot for each HUT. The time axis is labelled at the top and bottom. The units are major frames (40.96 sec). For some obscure reason, when

1) To determine secular variability, weak sources are subjected to the NU**2 test, and stronger sources are subjected to a chi-squared test
2) Tests for periodic variability are applied for all sources with 20 or more counts above background. ("Fourier Analysis")

Parameters for the Fourier Analysis for this field are:

elapsed time:last photon arrival
- first photon arrival = 1201.0 secs
# of frequency bins = 8192
minimum period tested = .147 secs
maximum period tested = 1200.960 secs
minimum frequency tested = .83267E-03 Hz
maximum frequency tested = .68212E 01 Hz

In the following table, the first line for each source is based on the distribution of arrival times, and the second line is based on the distribution of intervals between arrivals.

SOURCE	CTS	SECULAR TESTS					PERIODIC TESTS				
		NU**2	PROB	CHI-SQ	DOF	PROB	FOURIER COEFF	PROB	PERIOD (SECS)	FREQ (HZ)	FREQ BIN
1	147.			21.139	19	.3292	3.16	.3259	.260E 00	3.85	4620
				17.115	19	.5821					
2	21.	.155	.3937				2.87	.9124	.328E 00	3.05	3664
		.124	.4741								
3	9.	.149	.4080								
		.063	.6854								
4	7.	.189	.3208								
		.028	.8441								

The probabilities listed for the secular tests refer to the probability that the source is constant. Only if PROB < 0.1, should you start thinking seriously about the possibility of variability.
The PROBability associated with the Fourier Analysis is the probability that a steady source would yield the fourier coefficient listed.

10 major frames have elapsed, there appears the label "1280" which is the minor frame count (128 minor frames = 1 major frame). The tiny ticks are 1/8 of a major frame (42 secs).

When a star tracker is locked on to a guide star, the "U (and V) STA A" should show a constant trace; and the separation (between guide stars) should also be relatively constant. U and V are the coordinates of the star trackers. Tracker B failed soon after launch. A saw tooth (interrupted) pattern indicates a scanning mode from which Aspect (via MAPMODE) can often be achieved. The RGA strips give data from the gyros, deviations from a horizontal line indicating momentum transfers to the satellite ("tweeking up" the pointing).

The second set of strip charts give various counting rates, as labelled. VALID(SS) means "valid secondary science" events which are the total HRI counts approved by on-board discriminators. INVALID(SS) are those events rejected by on-board discriminators. The "Total HRI" are the fraction of VALID(SS) which actually contribute to the image. MPC PSD gives the Pulse Shape Discriminator output for the Monitor Proportional Counter. Larger values correspond to a higher fraction of particles to photons. SAAD (1 and 2) are the South Atlantic Anomaly Detectors (excess charged particles) and BOD stands for "Bright Object Detector" (usually the Earth; at least once, the Moon).

4.10 Conversion of Count Rate to Flux

The effective area of the HRI as a function of energy is shown in figure 4.10.0. This figure and all the subsequent discussion below is for "HRI-3". HRI-2 had a thicker window and was used for a few observations at the beginning of the mission. Since no spectral information is recorded for HRI counts, it is quite clear that sources of identical flux in a given band may give vastly different count rates depending on their spectral distribution. A further complication arises because the point response function PRF varies both with photon energy, E, and with radial distance, R, from the field center.

The only way to convert a count rate to flux is to have some a priori notion of the spectral distribution. The highest accuracy is obtained by using the program HXLUM (described elsewhere in the UM) which folds your choice of spectrum with the effective area, correcting for scattering with the appropriate PRF(E,R), finally matching the results with the observed count rate. The flux density at any E or the flux over a specified band from the calculated incident spectrum is then known.

In the standard reductions (production run PRD) correction factors for the photons which fell outside the standard circle of radius = 18 arcsec were applied as a function of R. However, since the spectral distribution was unknown, we had to make the scattering (and vignetting) correction for a particular energy (1 keV). The "final" result from PRD was a count rate:

NET/1000 = (cts-BG)*DTC*QEC*SCSC*VIG*1000/EXP

For the convenience of users, we have prepared a set of tables and figures which give the conversion factors for various types of spectra:

Flux = CF*(NET/1000)
(or Flux density)
where CF = conversion factor (the entries in the tables)

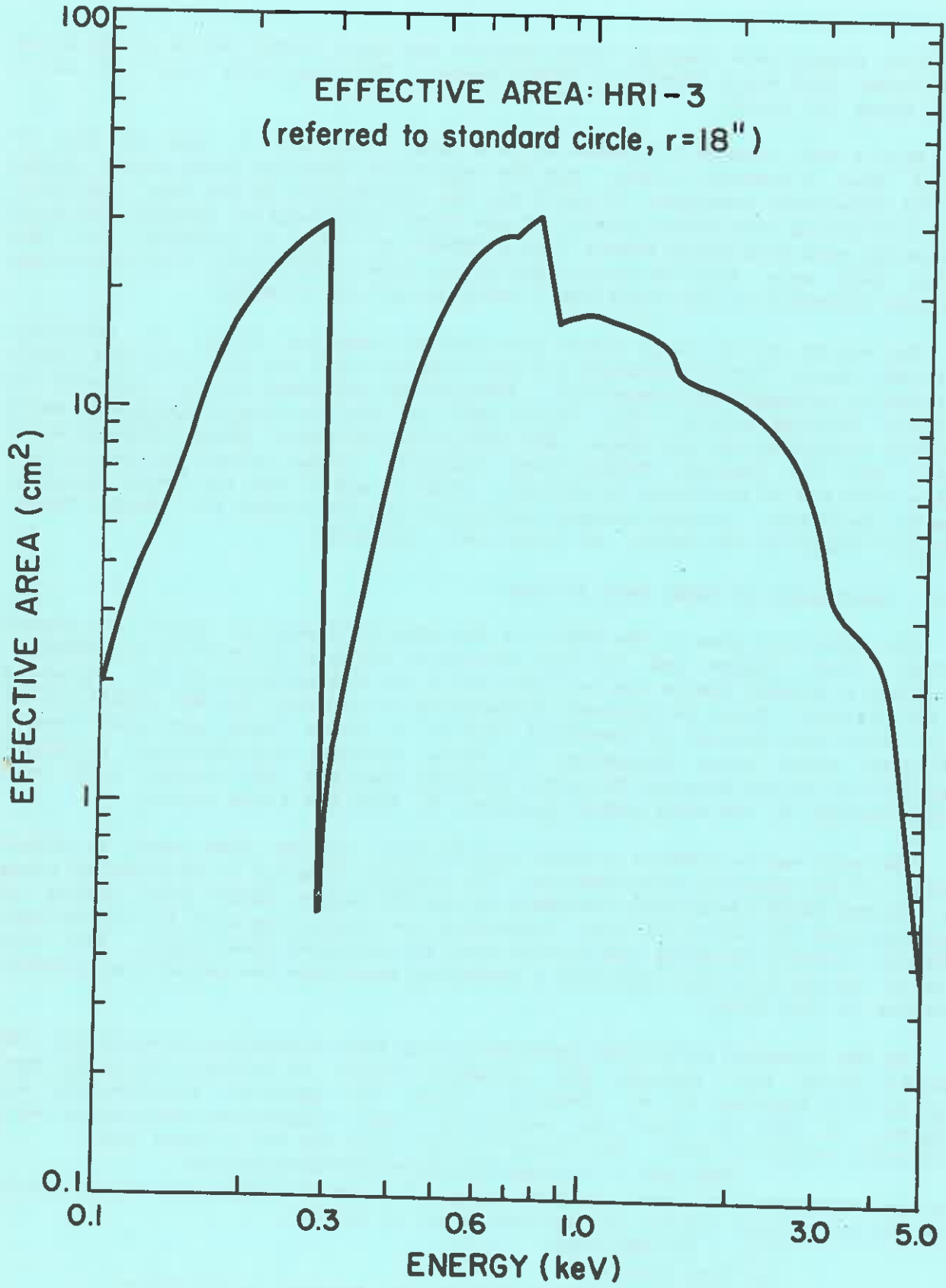
EFFECTIVE AREA: HRI-3
(referred to standard circle, r=18")
EFFECTIVE AREA (cm²)
100
10
1
0.1
0.1
0.3
0.6
1.0
3.0
5.0
ENERGY (keV)

Figure 4.10.0

and Fluxes are in cgs units.

The Tables were prepared by running HXLUM (May 82) for a source at the field center of intensity 0.7924 counts for an observation of 1000 seconds. The 1 keV scattering correction is 1.262, so we have "uncorrected" your value of NET/1000 by this factor in order that the correct usage of SC(E,R=0) can be folded with your chosen spectral distribution by HXLUM. Since the conversion tables are already multi-dimensional, we have not tried to incorporate SC(R). Please note, that your PRD (NET/1000) value, while automatically being "uncorrected" for SC(E), maintains (to first order) its SC(R). It is only "to first order" because the E and R dependency are not separable.

The current set of tables includes:

Table 1: Observed Flux: 0.15-1.5 keV (the soft band, closest to that observed)
2: Emitted Flux: 0.15-1.5 keV
3: Observed Flux: 0.2-4.0 keV (the broad "EO" band)
4: Emitted Flux: 0.2-4.0 keV
5: Observed Flux Density: at 1 keV (soft, but normally not heavily absorbed)
6: Emitted Flux Density

4 Spectral Types:

A) Power law, with photon number index
B) Exponential plus Gaunt
C) Raymond Thermal
D) Black Body

Care should be taken when using the Figures (particularly for the Raymond Spectrum) since the curves were drawn free-hand and sharp features may have been overlooked.

As an example, suppose we wish to estimate the flux and flux density of Source 1 (List 4.3): NET/1000 = 218. For a power law with photon number index $\alpha = 2$ and $N_H = 10^{21}\ cm^{-2}$, we find CF = 1.17E-13 in Table 3A (or Figure 3A) for the observed flux in the 0.2-4 keV band.

F = Flux = CF*(NET/1000) = 2.5E-11 erg $cm^{-2}s^{-1}$. /(3.8 keV) $\Delta E =$

The observed flux density, S, at 1 keV is found from Table 5A (Figure 4.10/5A).

$S = 2.06E-31*218 = 4.47E-29$ erg $cm^{-2}s^{-1}Hz^{-1}$.

$= 4.47E-3$ mJy

DIVIDING F by 3.8 and by the CF $1\ mJy = 2.42\times10^{-9}$ erg cm^{-2} keV^{-1} s^{-1}

$\Rightarrow S \sim 2.72\times10^{-3}$ mJy $\equiv Z$

$\frac{C_5\times10^{26}}{CF} \times Z = 0.426 \Rightarrow (\Delta E)_{band} \sim 2.35$keV

TABLE 1A
OBSERVED FLUX: BAND 0.15-1.5 KEV

Log N_H	Power Law α 1.0	2.0	3.0	4.0
19	4.43E-14	3.19E-14	2.11E-14	1.49E-14
20	4.88E-14	4.02E-14	3.00E-14	2.32E-14
21	5.88E-14	5.83E-14	5.44E-14	5.17E-14
22	4.02E-14	5.63E-14	6.98E-14	7.79E-14
23	1.22E-16	2.58E-16	5.12E-16	9.55E-16

TABLE 2A
EMITTED FLUX: BAND 0.15-1.5
(CORRECTED FOR ABSORPTION IN GALAXY)

Log N_H	Power Law α 1.0	2.0	3.0	4.0
19	4.48E-14	3.27E-14	2.22E-14	1.61E-14
20	5.36E-14	4.98E-14	4.51E-14	4.28E-14
21	9.53E-14	1.41E-13	2.51E-13	5.23E-13
22	3.05E-13	8.93E-13	3.43E-12	1.61E-11
23	2.69E-12	1.40E-11	1.04E-10	1.02E-09

TABLE 3A
OBSERVED FLUX: BAND 0.2-4 KEV

Log N_H	Power Law α 1.0	2.0	3.0	4.0
19	1.26E-13	4.22E-14	1.72E-14	8.82E-15
20	1.47E-13	5.95E-14	2.94E-14	1.80E-14
21	2.32E-13	1.17E-13	7.15E-14	5.63E-14
22	5.01E-13	3.54E-13	2.49E-13	1.79E-13
23	1.13E-12	1.07E-12	9.82E-13	8.78E-13

TABLE 4A
EMITTED FLUX: BAND 0.2-4 KEV

Log N_H	Power Law α 1.0	2.0	3.0	4.0
19	1.26E-13	4.26E-14	1.76E-14	9.11E-15
20	1.51E-13	6.48E-14	3.57E-14	2.43E-14
21	2.68E-13	1.84E-13	1.99E-13	2.96E-13
22	8.58E-13	1.16E-12	2.72E-12	9.13E-12
13	7.57E-12	1.82E-11	8.25E-11	5.79E-10

TABLE 5A
OBSERVED FLUX DENSITY AT 1 KEV

Log N_H	Power Law α 1.0	2.0	3.0	4.0
19	1.37E-31	5.87E-32	1.53E-32	3.01E-33
20	1.61E-31	8.77E-32	3.05E-32	7.88E-33
21	2.37E-31	2.06E-31	1.40E-31	7.98E-32
22	1.17E-31	2.00E-31	2.95E-31	3.78E-31
23	7.64E-39	2.33E-38	6.55E-38	1.78E-37

TABLE 6A
EMITTED FLUX DENSITY AT 1 KEV
(CORRECTED FOR ABSORPTION IN GALAXY)

Log N_H	Power Law α 1.0	2.0	3.0	4.0
19	1.37E-31	5.88E-32	1.53E-32	3.02E-33
20	1.64E-31	8.95E-32	3.11E-32	8.05E-33
21	2.92E-31	2.54E-31	1.73E-31	9.82E-32
22	9.34E-31	1.60E-30	2.36E-30	3.03E-30
23	8.25E-30	2.51E-29	7.18E-29	1.92E-28

TABLE 1B
OBSERVED FLUX: BAND 0.15-1.5 keV

Log N_H	Exponential & Gaunt kT						
	0.03	0.08	0.15	0.3	1.0	3.0	30.0
19	7.19E-15	1.42E-14	1.89E-14	2.49E-14	3.54E-14	4.04E-14	4.28E-14
20	1.44E-14	1.97E-14	2.53E-14	3.22E-14	4.27E-14	4.68E-14	4.81E-14
21	2.52E-14	4.99E-14	5.05E-14	5.17E-14	5.90E-14	6.12E-14	5.99E-14
22	4.44E-14	4.82E-14	7.06E-14	8.74E-14	7.08E-14	5.54E-14	4.44E-14
23	1.11E-13			5.01E-15	7.06E-16	2.80E-16	1.51E-16

TABLE 2B
EMITTED FLUX: BAND 0.15-1.5
(CORRECTED FOR ABSORPTION IN GALAXY)

Log N_H	Exponential & Gaunt kT						
	0.03	0.08	0.15	0.3	1.0	3.0	30.0
19	8.12E-15	1.55E-14	2.01E-14	2.60E-14	3.62E-14	4.11E-14	4.33E-14
20	4.48E-14	4.09E-14	4.24E-14	4.54E-14	5.12E-14	5.35E-14	5.36E-14
21	1.08E-11	1.35E-12	4.69E-13	2.25E-13	1.35E-13	1.15E-13	1.03E-13
22	8.11E-07	1.00E-9	6.22E-11	7.47E-12	1.17E-12	5.82E-13	3.76E-13
23	8.30E+06			3.10E-09	4.49E-11	9.62E-12	3.87E-12

TABLE 3B
OBSERVED FLUX: BAND 0.2-4 keV

Exponential & Gaunt

Log N_H	kT						
	0.03	0.1	0.3	1.0	3.0	10.0	30.0
19	1.32E-15	9.19E-15	2.04E-14	3.93E-14	6.50E-14	8.84E-14	9.99E-14
20	4.44E-15	1.62E-14	2.97E-14	5.01E-14	8.05E-14	1.07E-13	1.20E-13
21	2.49E-14	5.12E-14	5.32E-14	7.66E-14	1.34E-13	1.77E-13	1.96E-13
22	4.61E-14	5.65E-14	1.16E-13	2.32E-13	3.50E-13	4.28E-13	4.58E-13
23	1.13E-13	2.04E-13	4.24E-13	8.79E-13	1.05E-12	1.10E-12	1.11E-12

TABLE 4B
EMITTED FLUX: BAND 0.2-4 keV

Exponential & Gaunt

Log N_H	kT						
	0.03	0.1	0.3	1.0	3.0	10.0	30.0
19	1.39E-15	9.54E-15	2.08E-14	3.97E-14	6.54E-14	8.88E-14	1.00E-13
20	7.67E-15	2.30E-14	3.64E-14	5.62E-14	8.50E-14	1.11E-13	1.24E-13
21	1.85E-12	5.00E-13	1.80E-13	1.35E-13	1.83E-13	2.20E-13	2.37E-13
22	1.39E-07	1.91E-10	5.99E-12	1.29E-12	9.26E-13	8.78E-13	8.71E-13
23	1.42E+06	3.07E-05	2.49E-09	4.29E-11	1.53E-11	1.01E-11	8.94E-12

TABLE 5B
OBSERVED FLUX DENSITY AT 1 keV

Exponential & Gaunt

Log N_H	kT						
	0.03	0.08	0.15	0.3	1.0	3.0	30.0
19	2.77E-43	1.05E-35	1.12E-33	1.40E-32	6.92E-32	1.05E-31	1.24E-31
20	1.50E-42	2.72E-35	2.33E-33	2.40E-32	9.61E-32	1.34E-31	1.51E-31
21	3.00E-40	7.43E-34	2.13E-32	9.84E-32	2.09E-31	2.39E-31	2.39E-31
22	3.46E-36	8.52E-32	4.35E-31	5.03E-31	2.81E-31	1.86E-31	1.35E-31
23	2.62E-31			1.55E-36	7.95E-38	2.28E-38	1.03E-38

TABLE 6B
EMITTED FLUX DENSITY AT 1 keV
(Corrected for absorption in the Galaxy)

Exponential & Gaunt

Log N_H	kT						
	0.03	0.08	0.15	0.3	1.0	3.0	30.0
19	2.77E-43	1.05E-35	1.13E-33	1.40E-32	6.93E-32	1.05E-31	1.24E-31
20	1.53E-42	2.78E-35	2.37E-33	2.45E-32	9.81E-32	1.37E-31	1.54E-31
21	3.69E-40	9.15E-34	2.62E-32	1.21E-31	2.58E-31	2.94E-31	2.95E-31
22	2.77E-35	6.82E-31	3.48E-30	4.03E-30	2.25E-30	1.49E-30	1.08E-30
23	2.83E-22			1.67E-27	8.59E-29	2.46E-29	1.11E-29

TABLE 1C
OBSERVED FLUX: BAND 0.15-1.5 keV

Log N_H	Raymond Thermal 10^6K							
	0.2	0.5	1.0	2.0	6.0	20.0	60.0	199.0
19	1.60E-15	6.49E-15	1.61E-14	2.86E-14	4.62E-14	5.35E-14	4.36E-14	4.27E-14
20	6.86E-15	1.56E-14	1.93E-14	3.31E-14	4.97E-14	6.52E-14	5.01E-14	4.86E-14
21	2.04E-14	1.11E-13	7.81E-14	5.00E-14	5.57E-14	8.03E-14	6.13E-14	5.78E-14
22	6.29E-14	5.22E-14	5.37E-14	6.96E-14	7.68E-14	8.38E-14	5.28E-14	4.48E-14
23	7.76E-14			1.83E-14	1.56E-15	8.72E-16	2.55E-16	1.82E-16

TABLE 2C
EMITTED FLUX: BAND 0.15-1.5 keV
(Corrected for Absorption in Galaxy)

Log N_H	Raymond Thermal 10^6K							
	0.2	0.5	1.0	2.0	6.0	20.0	60.0	199.0
19	1.87E-15	7.26E-15	1.75E-14	2.95E-14	4.66E-14	5.40E-14	4.42E-14	4.34E-14
20	3.19E-14	4.21E-14	3.93E-14	4.46E-14	5.35E-14	7.03E-14	5.61E-14	5.43E-14
21	9.01E-11	8.24E-12	1.85E-12	2.62E-13	8.91E-14	1.19E-13	1.06E-13	9.96E-14
22	1.04E-03	3.79E-8	9.53E-10	2.90E-11	1.35E-12	5.80E-13	4.43E-13	3.79E-13
23	2.82E+15			1.89E-07	2.84E-10	1.74E-11	5.56E-12	3.76E-12

TABLE 3C
OBSERVED FLUX: BAND 0.2-4 keV C_F

Log N_H	Raymond Thermal 10^6K						
	0.2	0.6	2.0	6.0	20.0	60.0	199.0
19	6.70E-17	4.11E-15	2.64E-14	4.72E-14	7.10E-14	8.30E-14	9.70E-14
20	6.31E-16	1.08E-14	3.20E-14	5.13E-14	8.88E-14	1.02E-13	1.18E-13
21	1.95E-14	1.01E-13	5.00E-14	5.87E-14	1.20E-13	1.59E-13	1.86E-13
22	6.29E-14	5.04E-14	7.21E-14	1.10E-13	2.42E-13	3.97E-13	4.62E-13
23	7.76E-14	1.49E-13	3.06E-13	5.95E-13	1.02E-12	1.14E-12	1.17E-12

TABLE 4C
EMITTED FLUX: BAND 0.2-4 keV

Log N_H	Raymond Thermal 10^6K						
	0.2	0.6	2.0	6.0	20.0	60.0	199.0
19	7.16E-17	4.32E-15	2.71E-14	4.75E-14	7.13E-14	8.34E-14	9.74E-14
20	1.22E-15	1.72E-14	4.09E-14	5.44E-14	9.26E-14	1.06E-13	1.22E-13
21	3.43E-12	2.47E-12	2.40E-13	9.05E-14	1.57E-13	2.02E-13	2.28E-13
22	3.95E-05	5.06E-09	2.66E-11	1.39E-12	7.97E-13	8.97E-13	9.19E-13
23	1.07E+14	1.69E+0	1.83E-07	3.28E-10	2.73E-11	1.25E-11	1.00E-11

TABLE 5C
OBSERVED FLUX DENSITY AT 1 keV C_S

Log N_H	Raymond Thermal 10^6K							
	0.2	0.5	1.0	2.0	6.0	20.0	60.0	199.0
19	0.0	7.57E-40	1.23E-35	1.85E-33	2.93E-31	5.73E-31	1.11E-31	1.18E-31
20	0.0	4.31E-39	2.71E-35	2.75E-33	3.30E-31	7.32E-31	2.38E-31	1.45E-31
21	0.0	6.99E-37	1.06E-33	1.34E-32	4.55E-31	1.02E-30	2.16E-31	2.21E-31
22	0.0	4.94E-34	8.39E-32	2.28E-31	1.06E-30	7.70E-31	1.39E-31	1.29E-31
23	0.0			1.10E-35	1.66E-36	1.71E-37	1.30E-38	9.51E-39

TABLE 6C
EMITTED FLUX DENSITY AT 1 keV
(Corrected for Absorption in the Galaxy)

Log N_H	Raymond Thermal 10^6K							
	0.2	0.5	1.0	2.0	6.0	20.0	60.0	199.0
19	0.0	7.59E-40	1.23E-35	1.86E-33	2.93E-31	5.74E-31	1.11E-31	1.18E-31
20	0.0	4.40E-39	2.77E-35	2.80E-33	3.37E-31	7.47E-31	1.41E-31	1.48E-31
21	0.0	8.61E-37	1.30E-33	1.65E-32	5.60E-31	1.26E-30	2.66E-31	2.72E-31
22	0.0	3.96E-33	6.71E-31	1.82E-30	8.49E-30	6.16E-30	1.11E-30	1.04E-30
23	0.0			1.19E-26	1.79E-27	1.85E-28	1.40E-29	1.03E-29

TABLE 1D
OBSERVED FLUX: BAND 0.15-1.5 keV

Log N_H	Black Body 10^6K						
	0.2	0.6	1.0	2.0	8.0	20.0	200.0
19	6.78E-15	1.95E-14	2.93E-14	4.43E-14	5.67E-14	4.34E-14	3.31E-14
20	1.40E-14	2.40E-14	3.48E-14	4.78E-14	5.76E-14	4.34E-14	3.30E-14
21	1.94E-14	5.41E-14	4.94E-14	5.62E-14	5.91E-14	4.13E-14	3.04E-14
22	4.83E-14	4.53E-14	6.57E-14	9.31E-14	3.85E-14	2.12E-14	1.41E-14
23	8.55E-14	9.78E-14	4.57E-14	6.53E-15	1.65E-16	4.78E-17	2.43E-17

TABLE 2D
EMITTED FLUX: BAND 0.15-1.5
(Corrected for Absorption in Galaxy)

Log N_H	Black Body 10^6K						
	0.2	0.6	1.0	2.0	8.0	20.0	200.0
19	7.71E-15	2.07E-14	3.03E-14	4.49E-14	5.69E-14	4.35E-14	3.32E-14
20	4.68E-14	4.08E-14	4.64E-14	5.32E-14	5.95E-14	4.46E-14	3.38E-14
21	2.08E-11	7.25E-13	2.21E-13	1.10E-13	7.60E-14	5.13E-14	3.72E-14
22	3.78E-05	4.86E-10	2.60E-11	1.82E-12	1.81E-13	8.80E-14	5.54E-14
23	3.00E+13	8.16E-3	1.16E-6	8.17E-10	2.03E-12	4.69E-13	2.16E-13

TABLE 3D
OBSERVED FLUX: BAND 0.2-4 keV

Log N_H	Black Body 10^6K						
	0.2	0.6	2.0	6.0	20.0	60.0	200.0
19	8.67E-16	1.36E-14	4.44E-14	1.54E-13	4.45E-13	5.60E-13	5.97E-13
20	3.11E-15	2.00E-14	4.86E-14	1.60E-13	4.54E-13	5.69E-13	6.05E-13
21	1.89E-14	5.43E-14	5.90E-14	1.97E-13	5.07E-13	6.18E-13	6.52E-13
22	4.98E-14	4.78E-14	1.22E-13	3.51E-13	7.08E-13	8.01E-13	8.26E-13
23	1.07E-13	1.35E-13	3.47E-13	9.71E-13	1.18E-12	1.15E-12	1.14E-12

TABLE 4D
EMITTED FLUX: BAND 0.2-4 keV

Black Body

Log N_H	10^6K						
	0.2	0.6	2.0	6.0	20.0	60.0	200.0
19	9.20E-16	1.41E-14	4.48E-14	1.54E-13	4.45E-13	5.60E-13	5.97E-13
20	5.59E-15	2.78E-14	5.31E-14	1.63E-13	4.56E-13	5.71E-13	6.06E-13
21	2.48E-12	4.93E-13	1.10E-13	2.21E-13	5.25E-13	6.34E-13	6.68E-13
22	4.51E-06	3.31E-10	1.81E-12	6.47E-13	9.01E-13	9.75E-13	9.95E-13
23	3.56E+12	5.55E-03	8.15E-10	1.15E-11	4.80E-12	4.07E-12	3.38E-12

TABLE 5D
OBSERVED FLUX DENSITY AT 1 keV

Black Body

Log N_H	10^6K						
	0.2	0.6	1.0	2.0	8.0	20.0	200.0
19	1.48E-49	1.17E-35	3.68E-33	1.03E-31	2.38E-31	1.66E-31	1.22E-31
20	8.82E-49	2.27E-35	5.55E-33	1.20E-31	2.34E-31	1.67E-31	1.22E-31
21	3.24E-46	3.34E-34	2.19E-32	2.05E-31	2.47E-31	1.59E-31	1.12E-31
22	9.08E-41	3.45E-32	3.96E-31	5.23E-31	9.06E-32	4.20E-32	2.55E-32
23	5.31E-31	4.29E-33	1.31E-34	1.74E-36	7.53E039	1.66E-38	7.40E-40

TABLE 6D
EMITTED FLUX DENSITY AT 1 keV
(Corrected for Absorption in the Galaxy)

Black Body

Log N_H	10^6K						
	0.2	0.6	1.0	2.0	8.0	20.0	200.0
19	1.48E-49	1.18E-35	3.69E-33	1.03E-31	2.28E-31	1.66E-31	1.23E-31
20	9.01E-49	2.32E-35	5.66E-33	1.22E-31	2.38E-31	1.70E-31	1.25E-31
21	3.99E-46	4.12E-34	2.69E-32	2.53E-31	3.04E-31	1.96E-31	1.37E-31
22	7.27E-40	2.76E-31	3.17E-30	4.18E-30	7.25E-31	3.36E-31	2.05E-31
23	5.73E-22	4.64E-24	1.41E-25	1.88E-27	8.13E-30	1.79E-30	7.99E-31

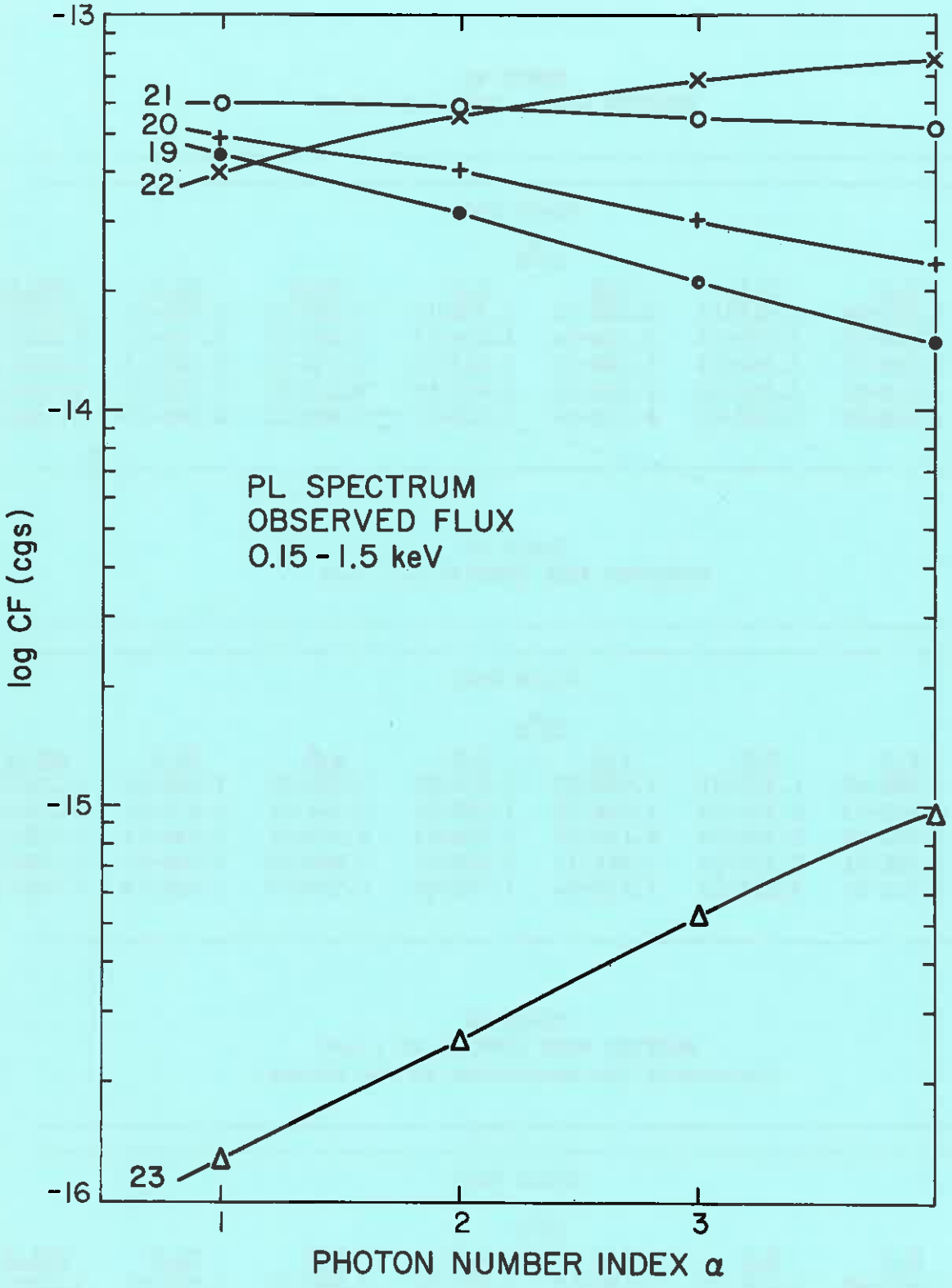

Figure 4.10.1A

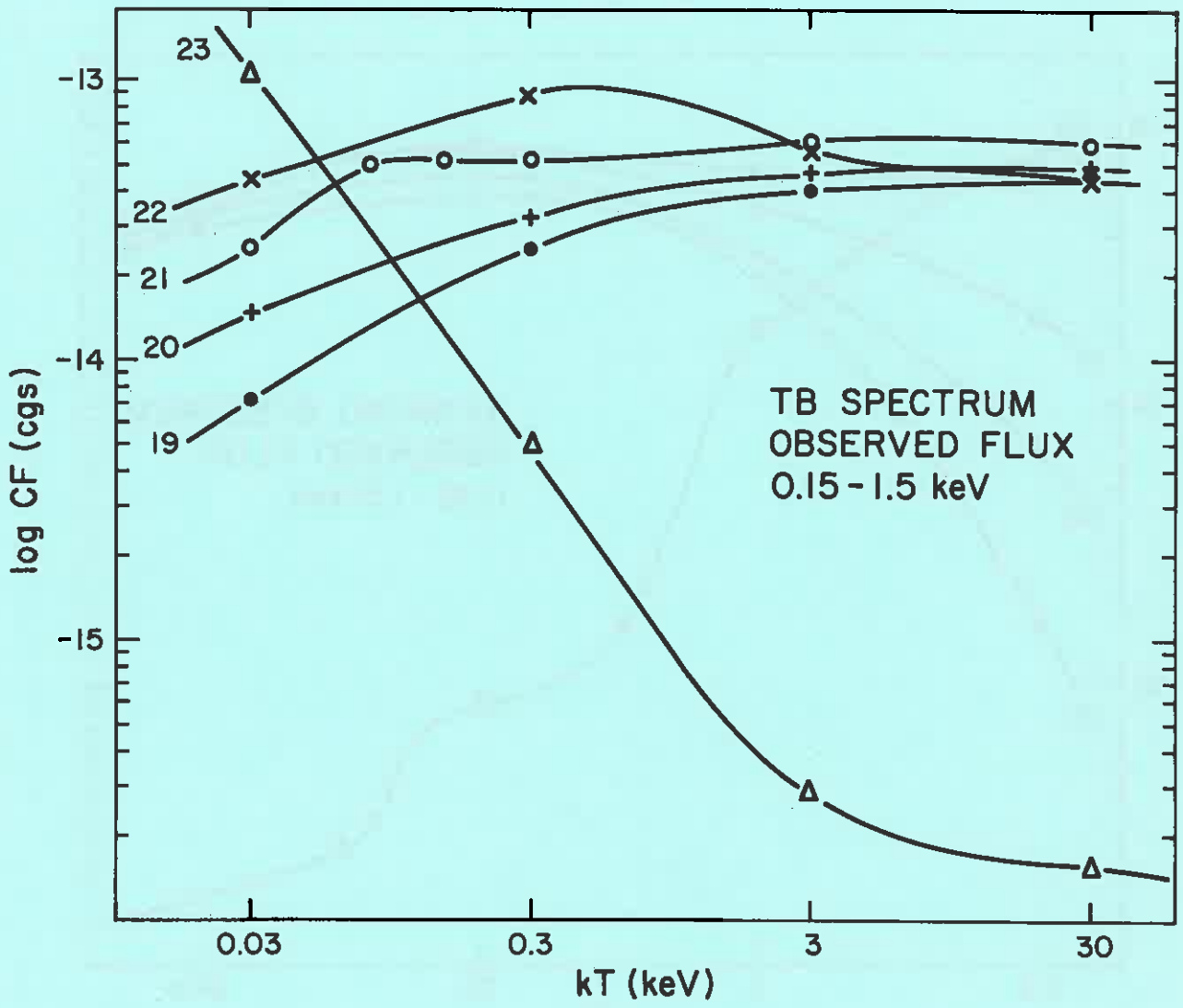

Figure 4.10.1B

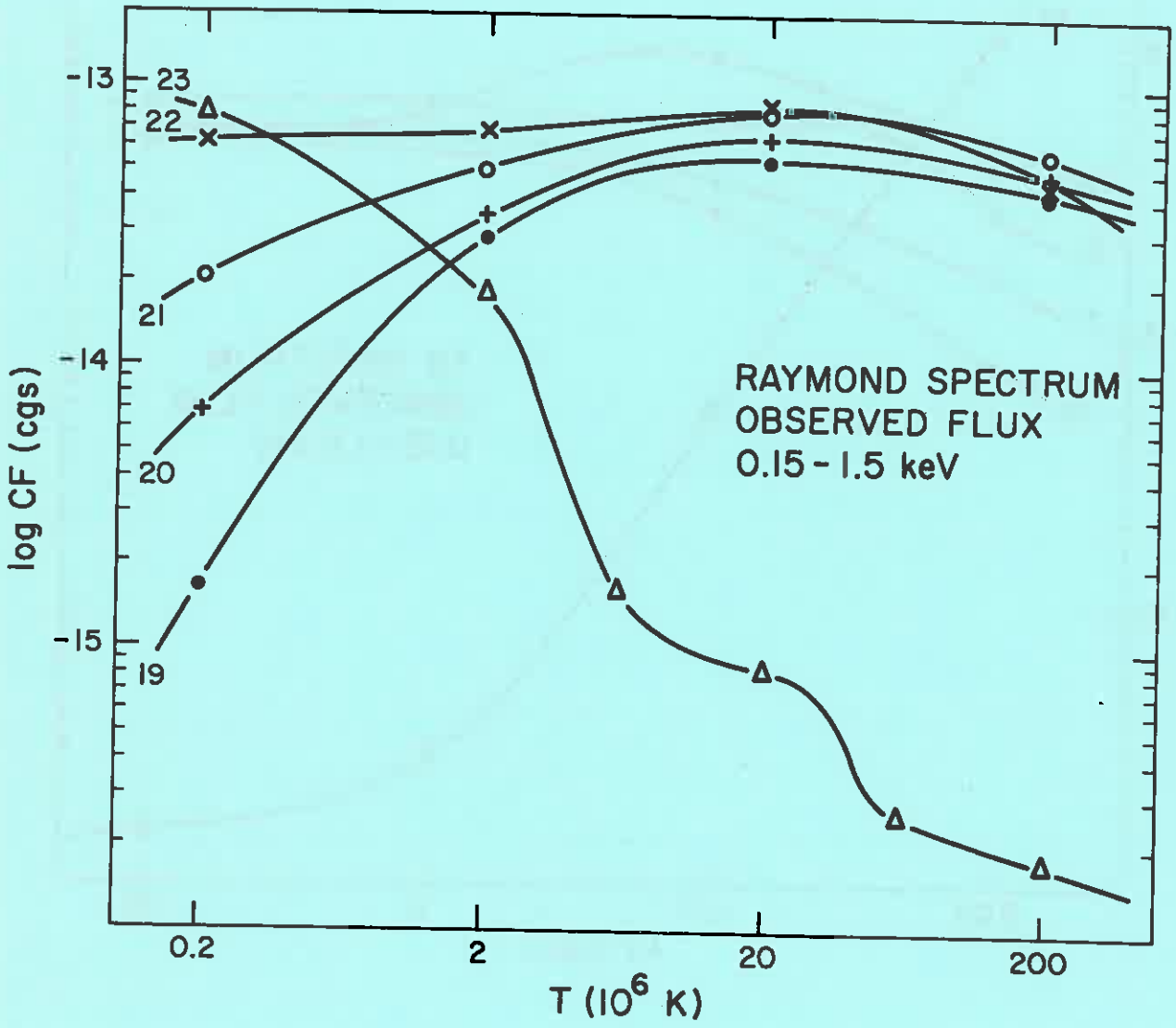

Figure 4.10.1C

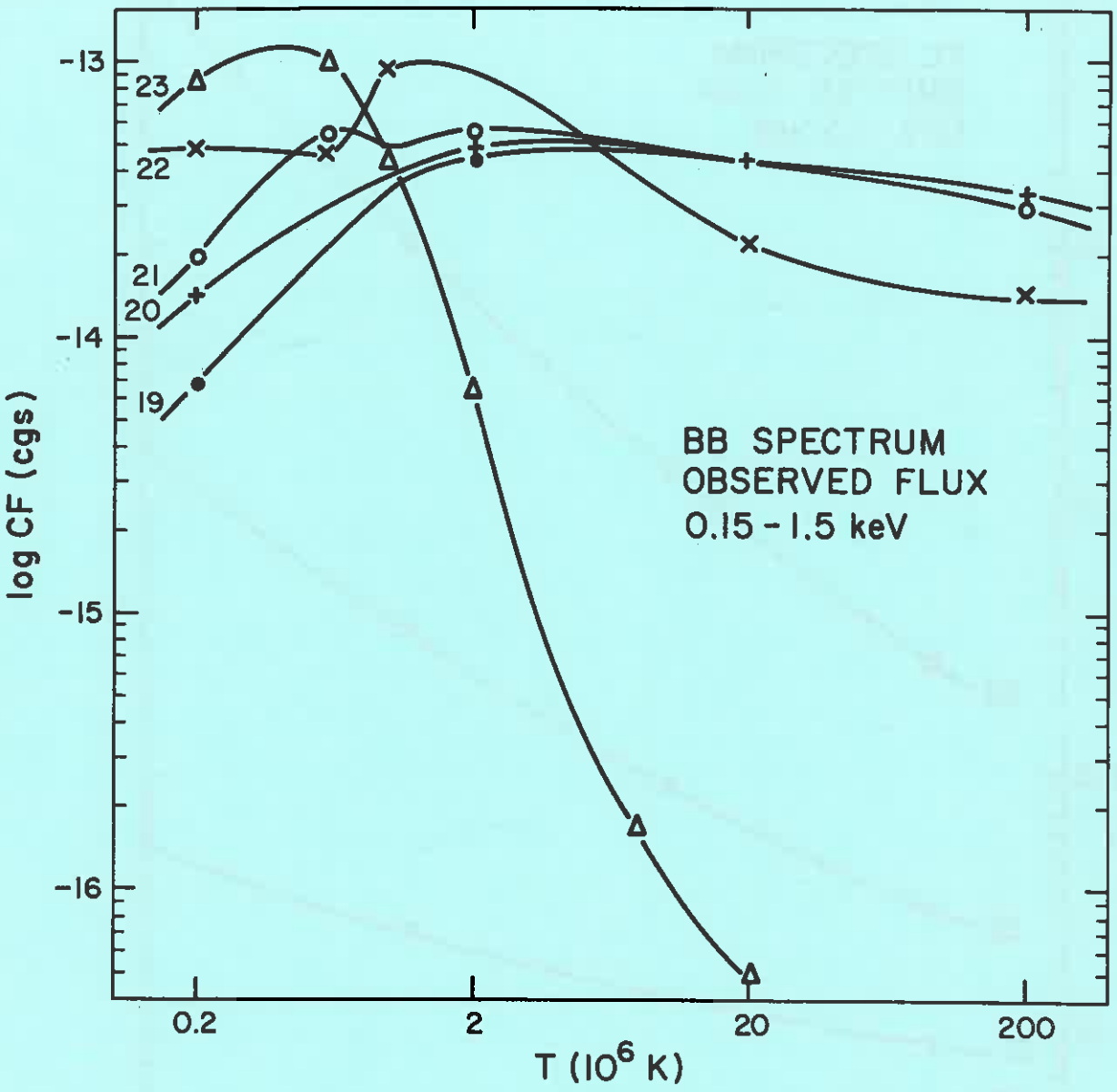

Figure 4.10.1D

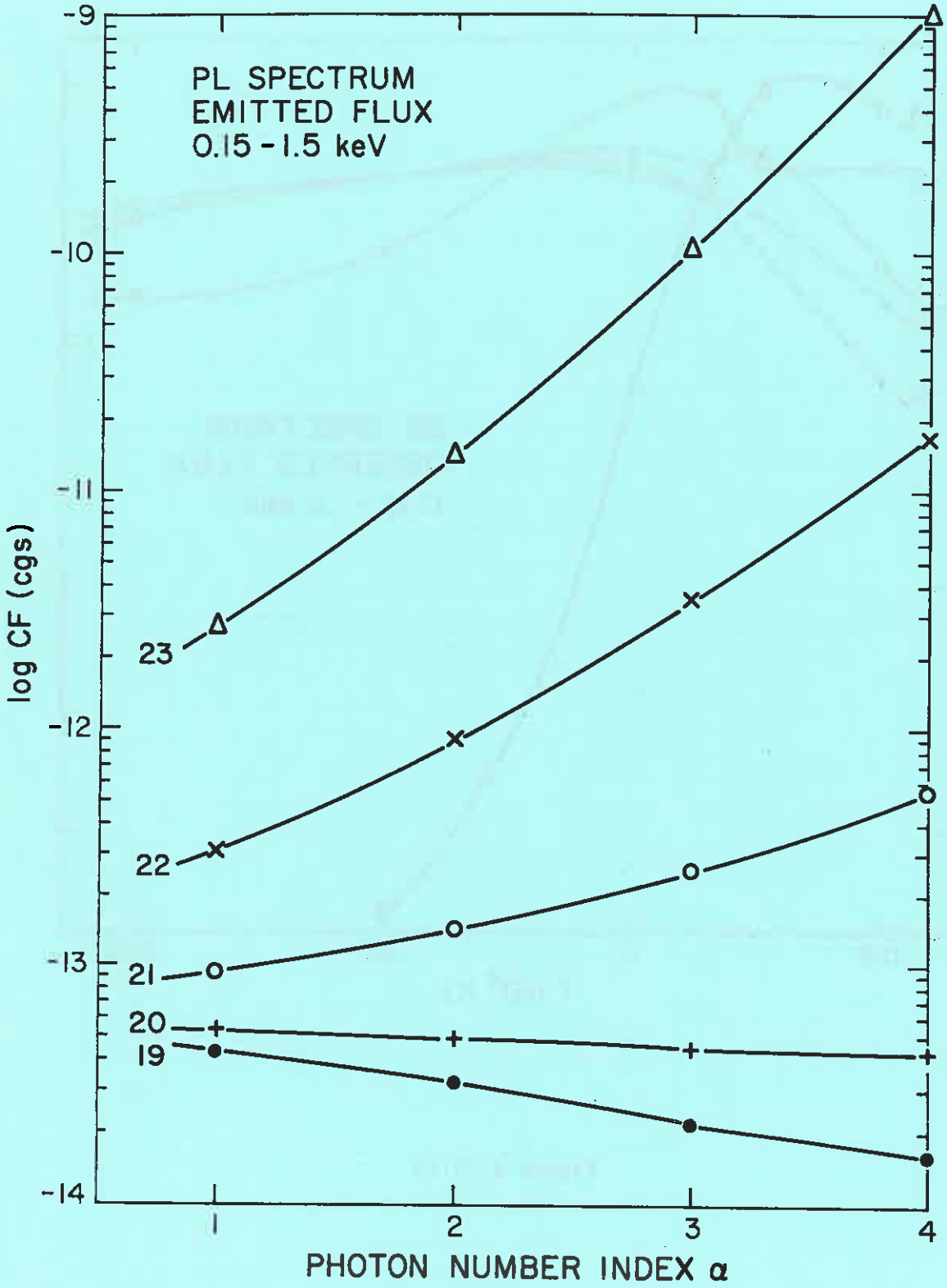

Figure 4.10.2A

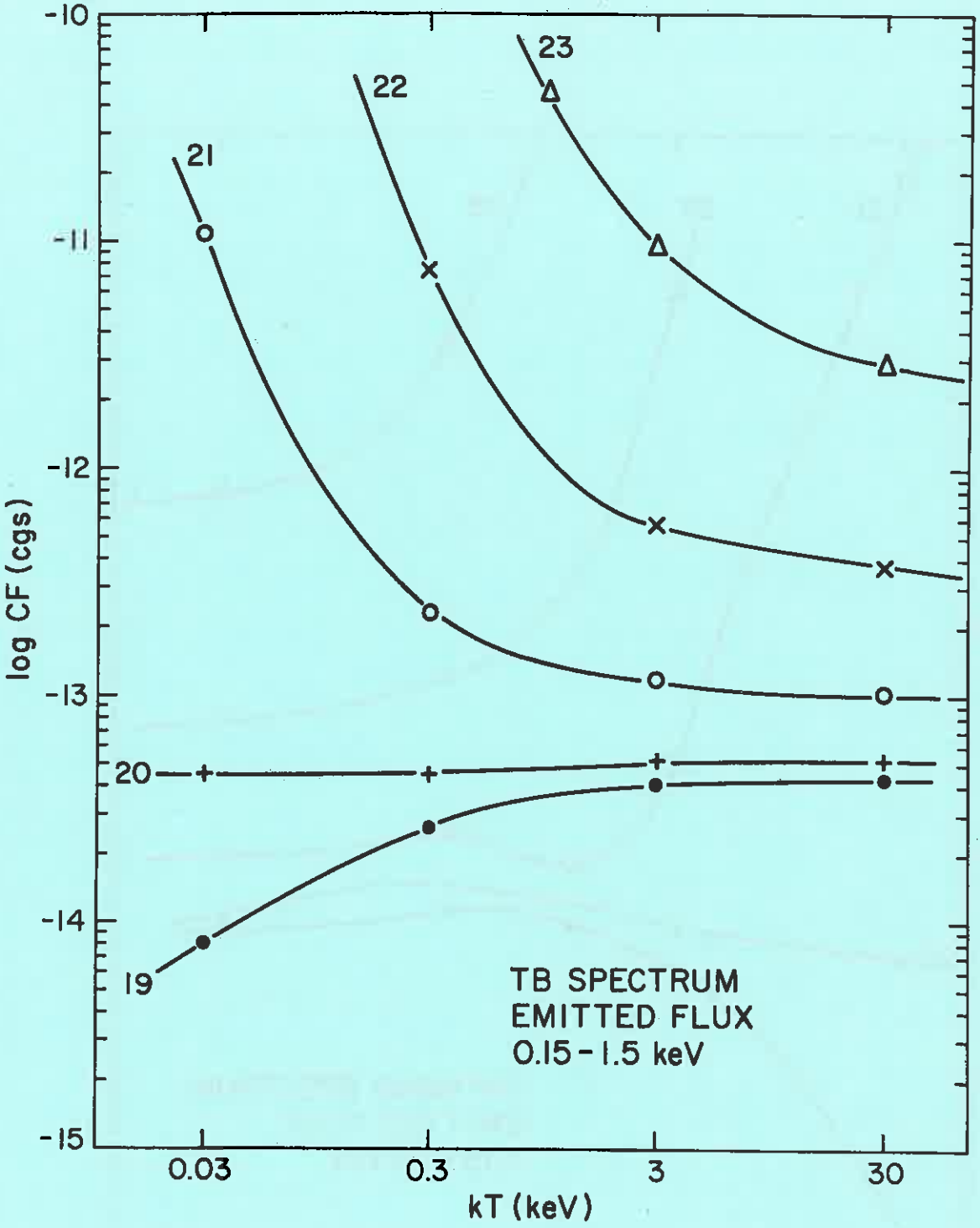

Figure 4.10.2B

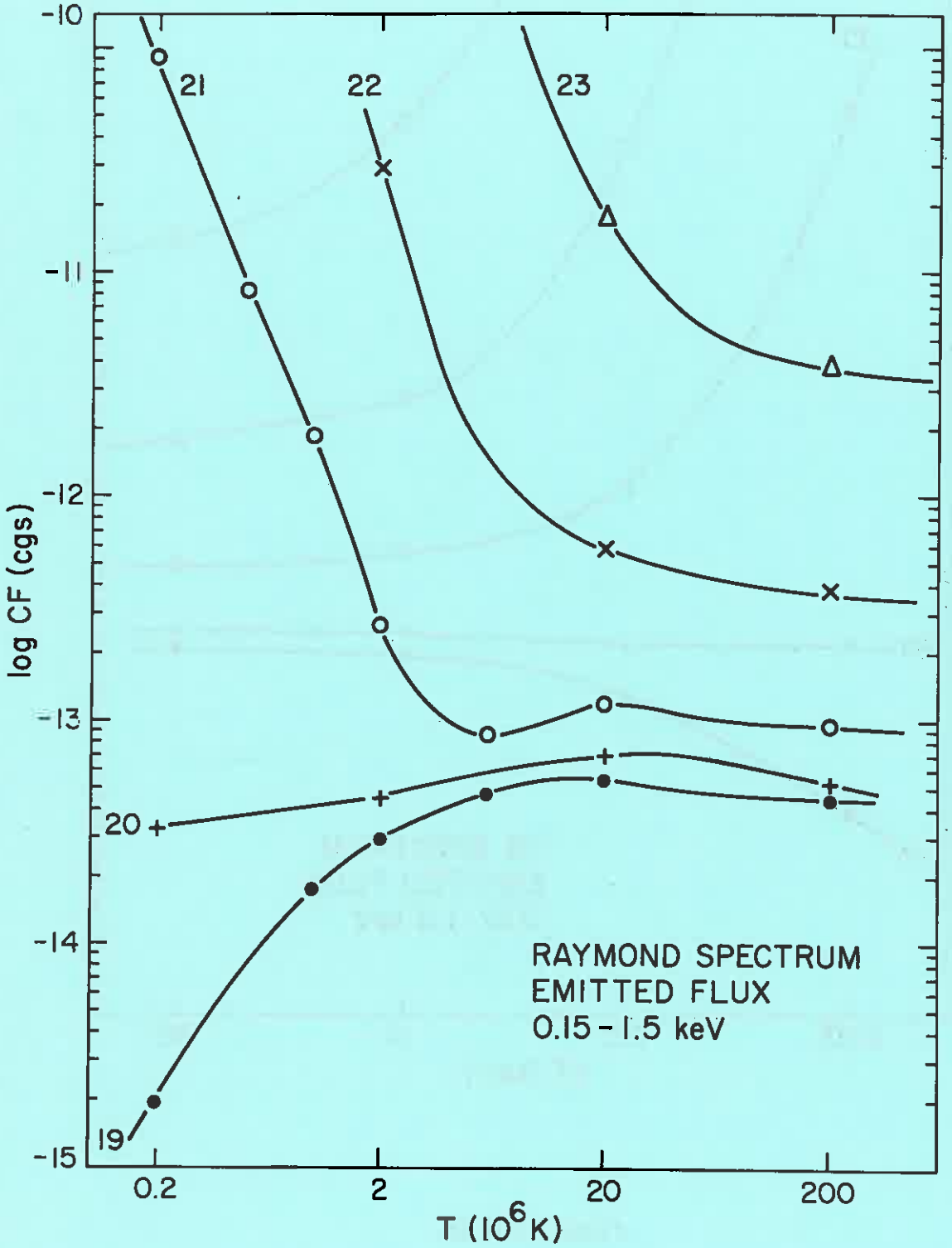

Figure 4.10.2C

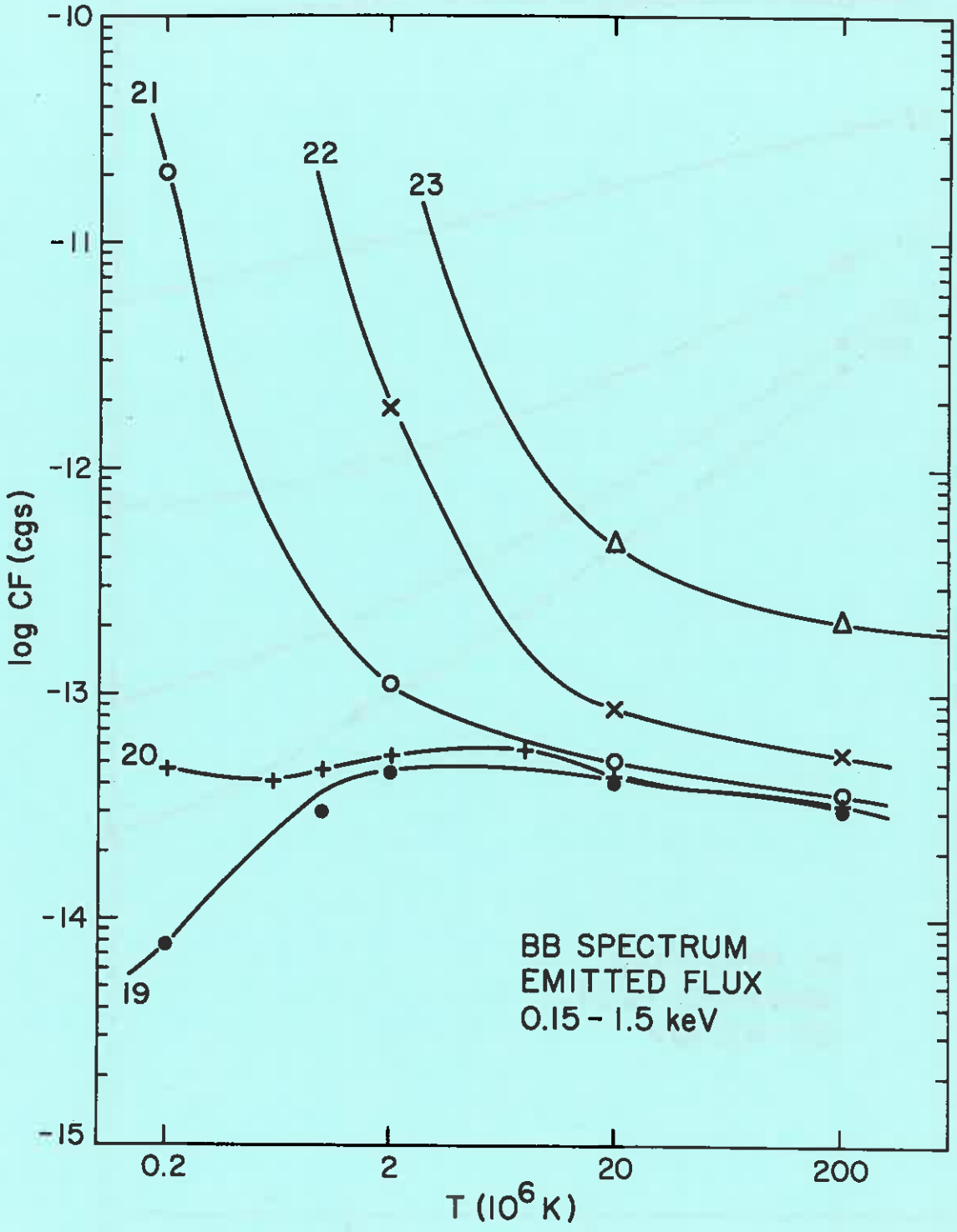

Figure 4.10.2D

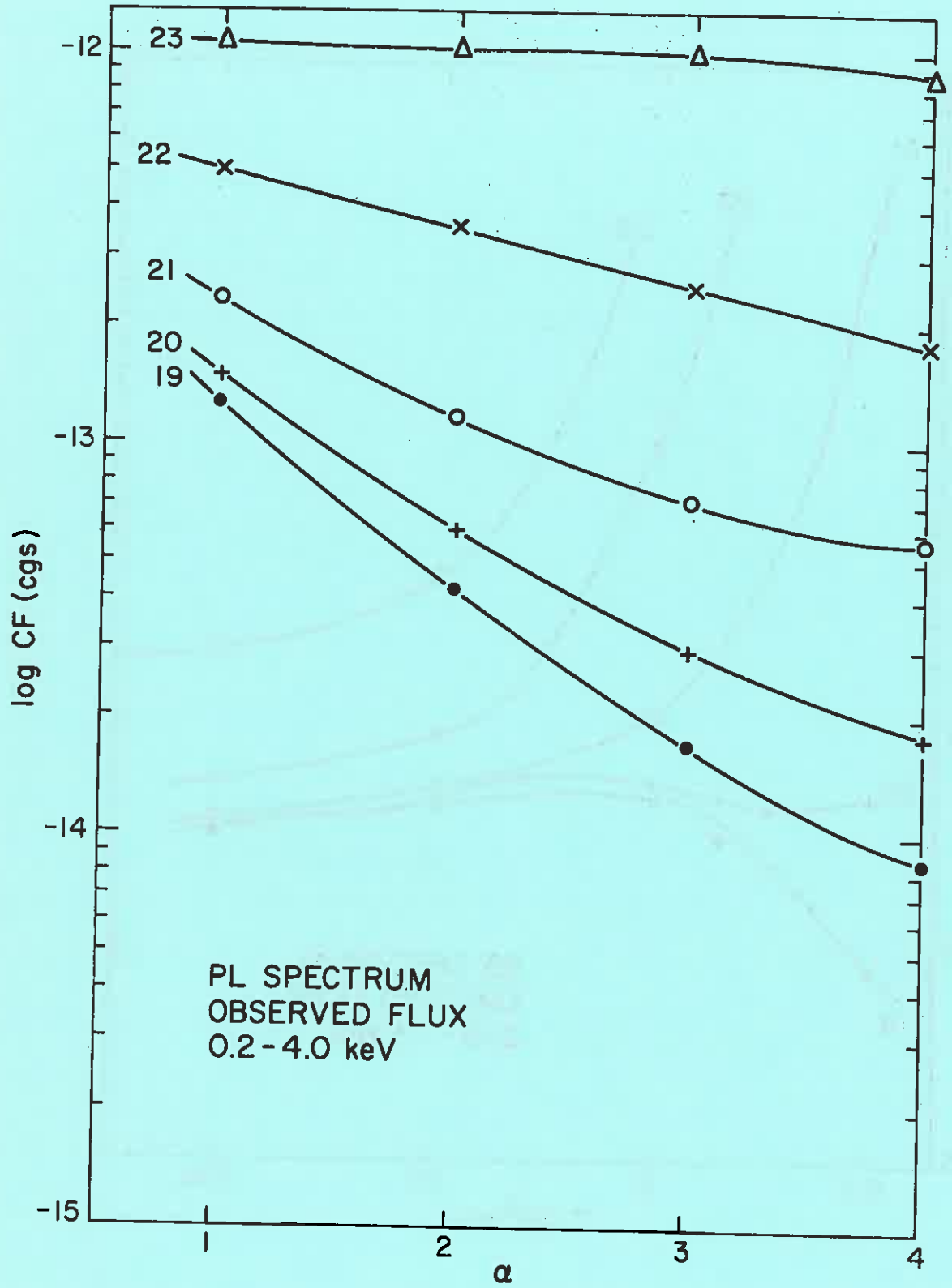

Figure 4.10.3A

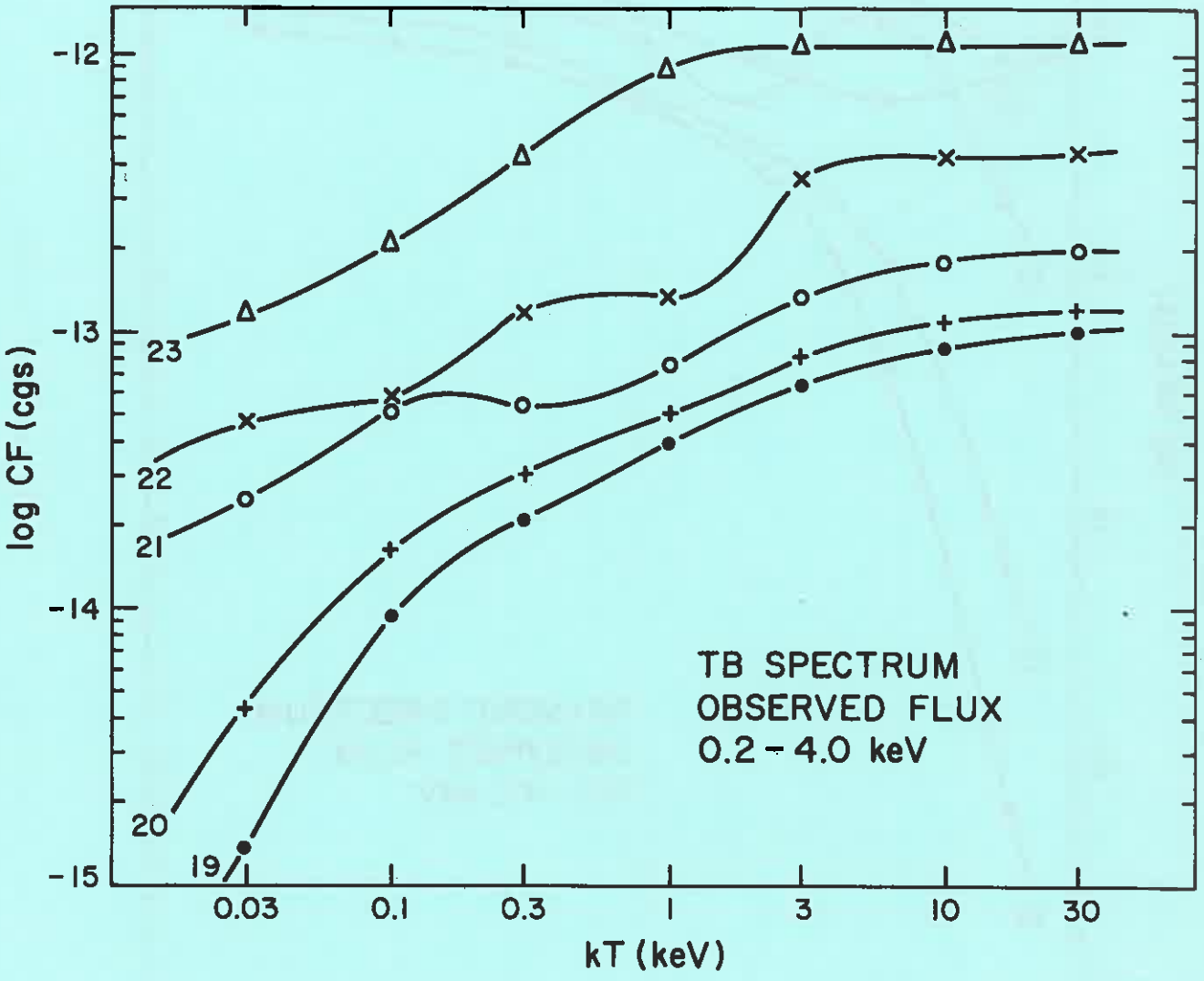

Figure 4.10.3B

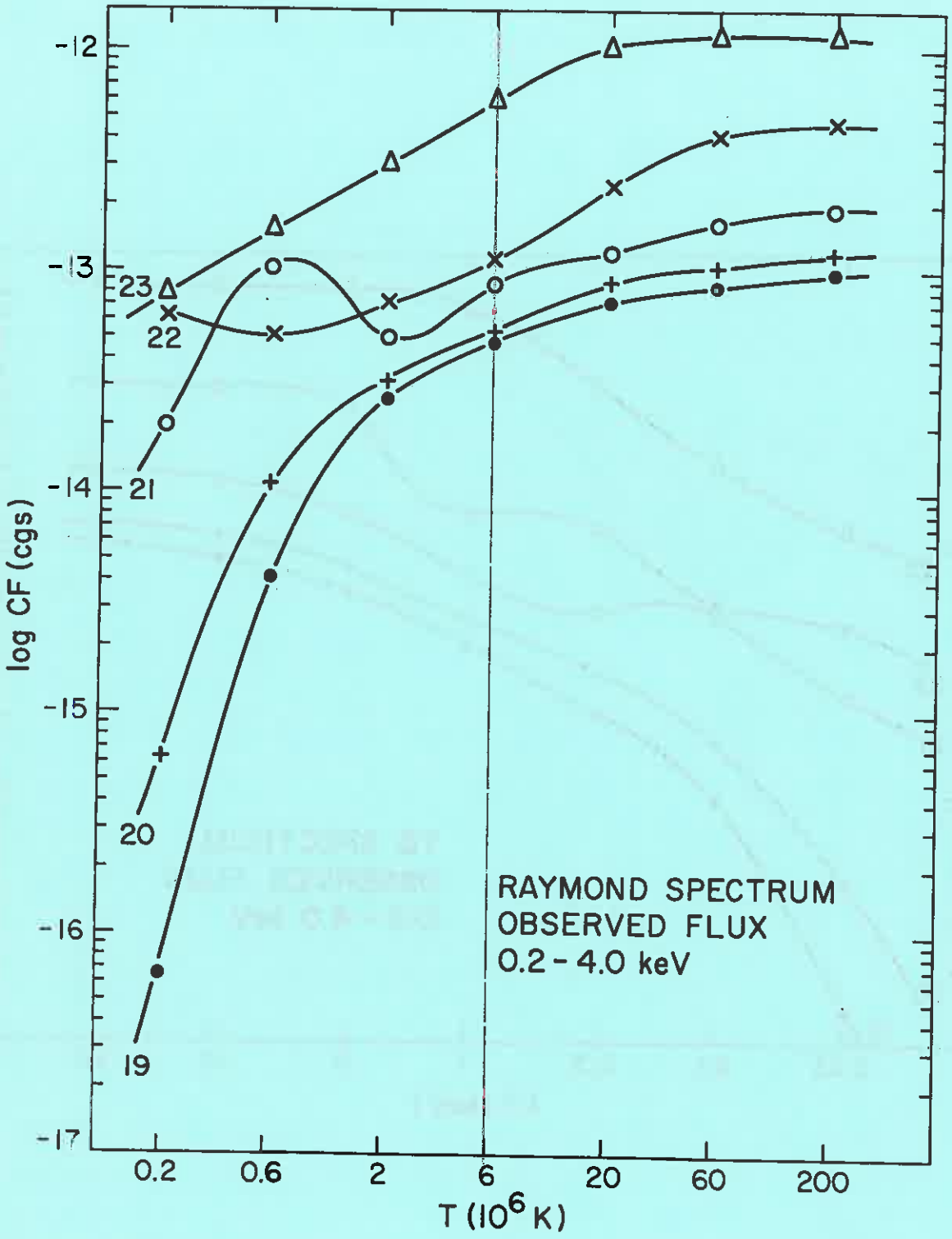

Figure 4.10.3C

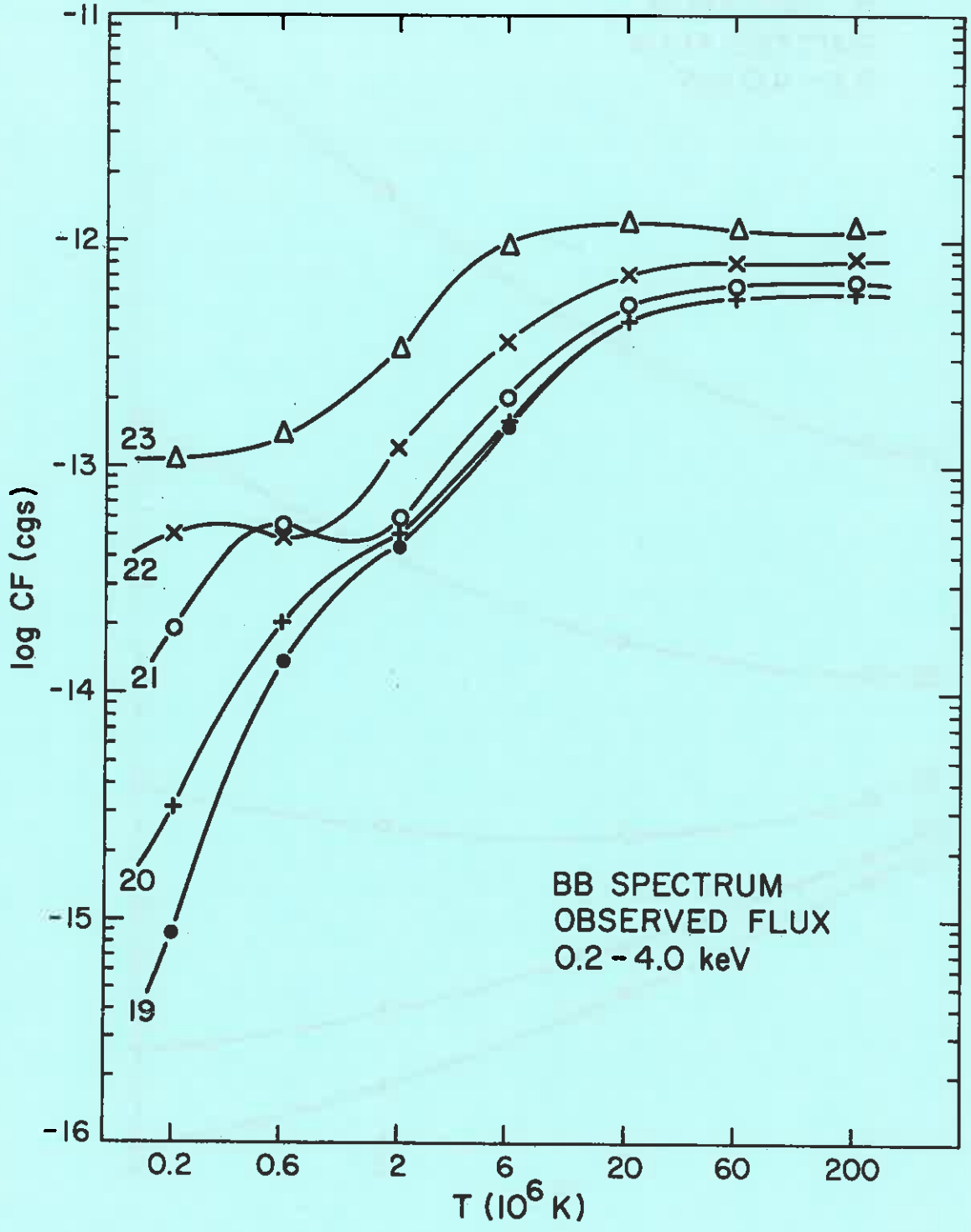

Figure 4.10.3D

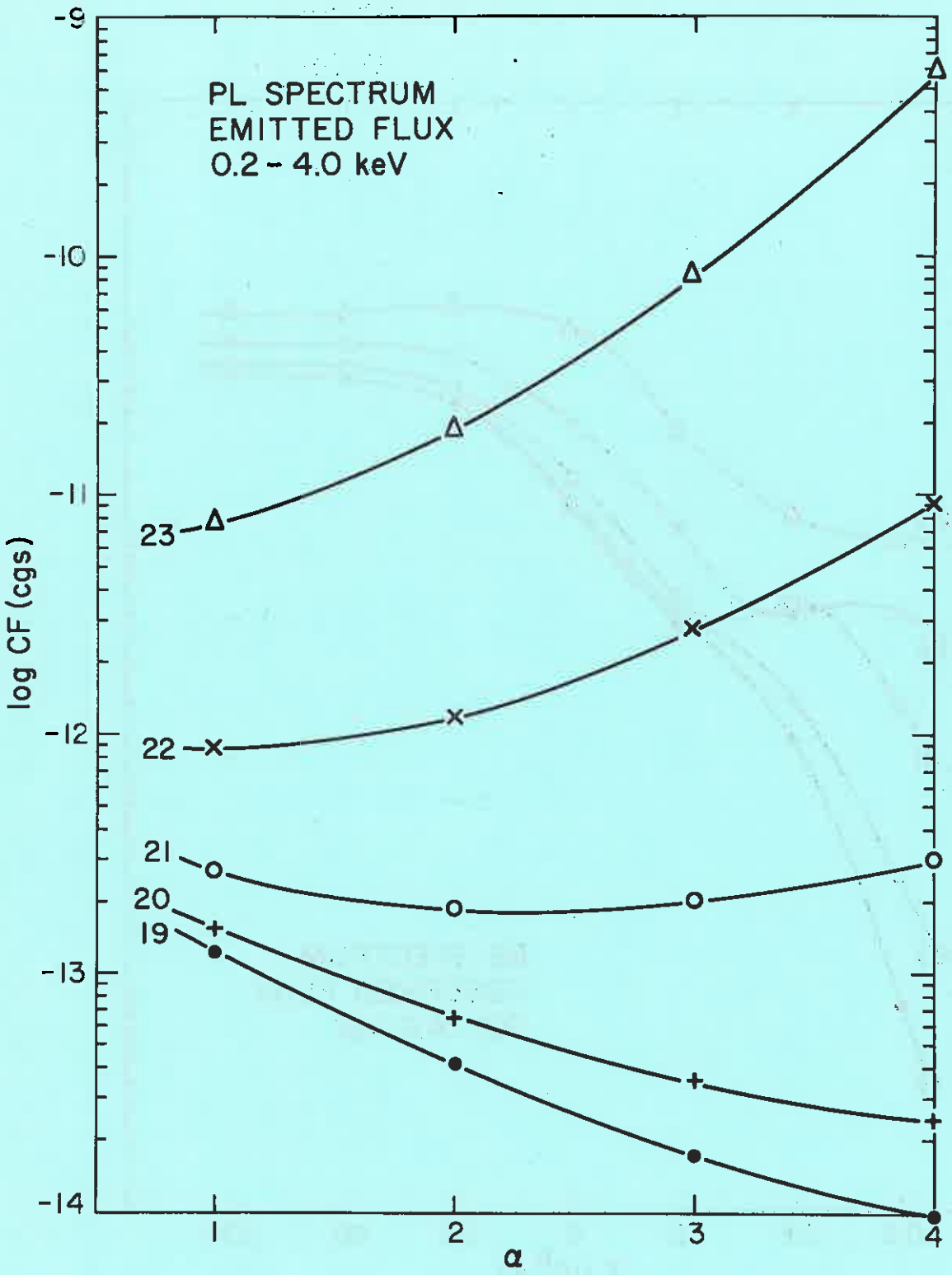

Figure 4.10.4A

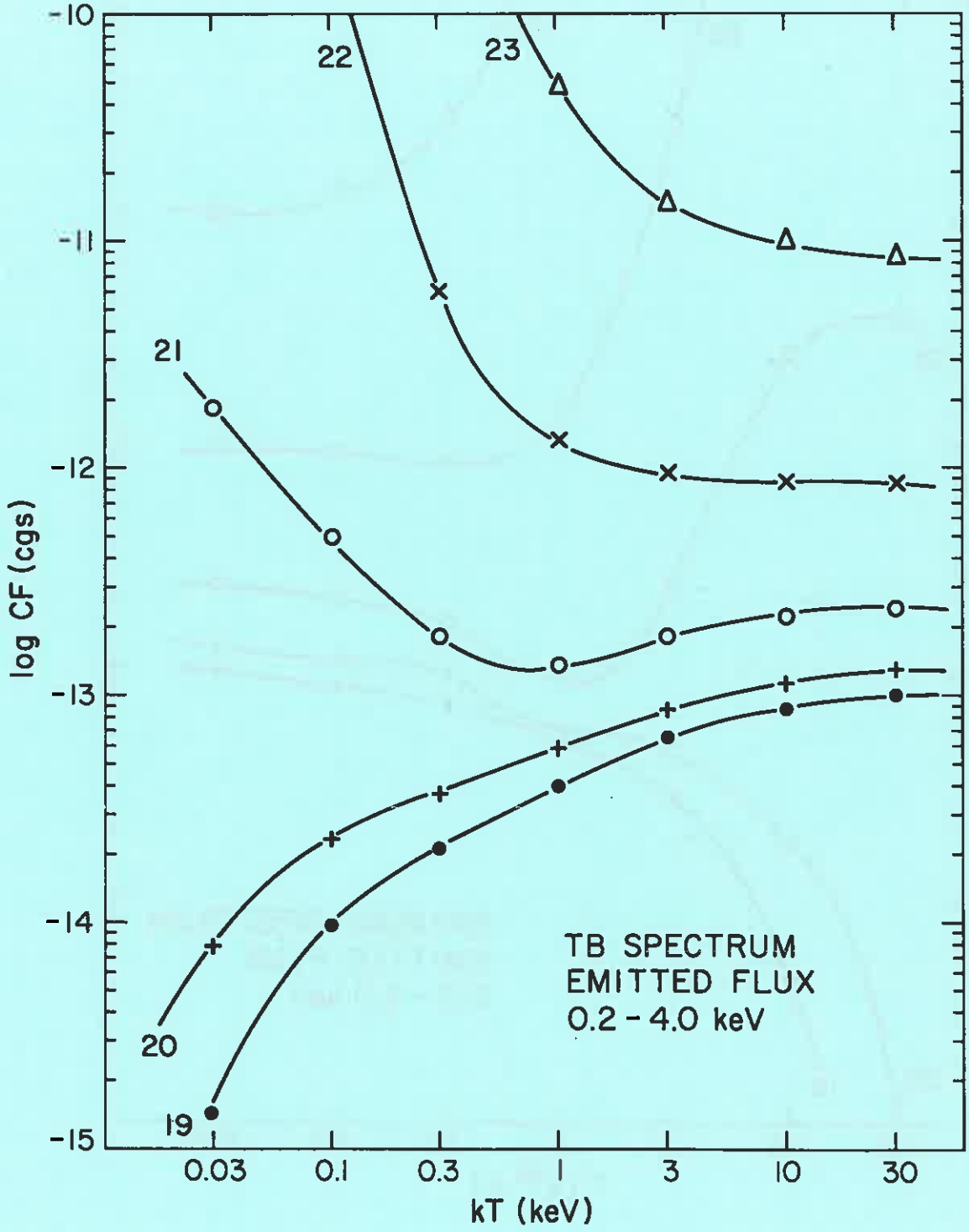

Figure 4.10.4B

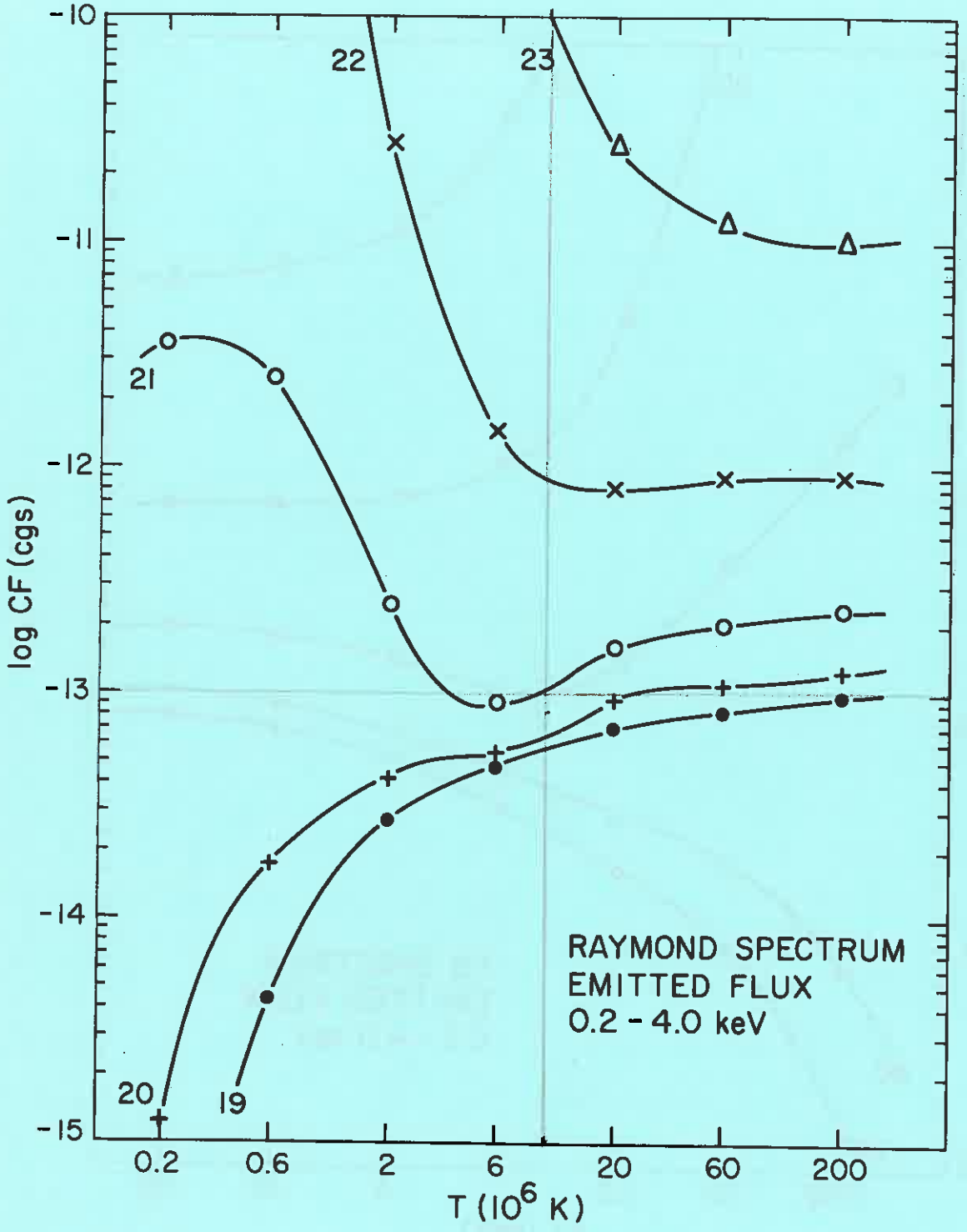

Figure 4.10.4C

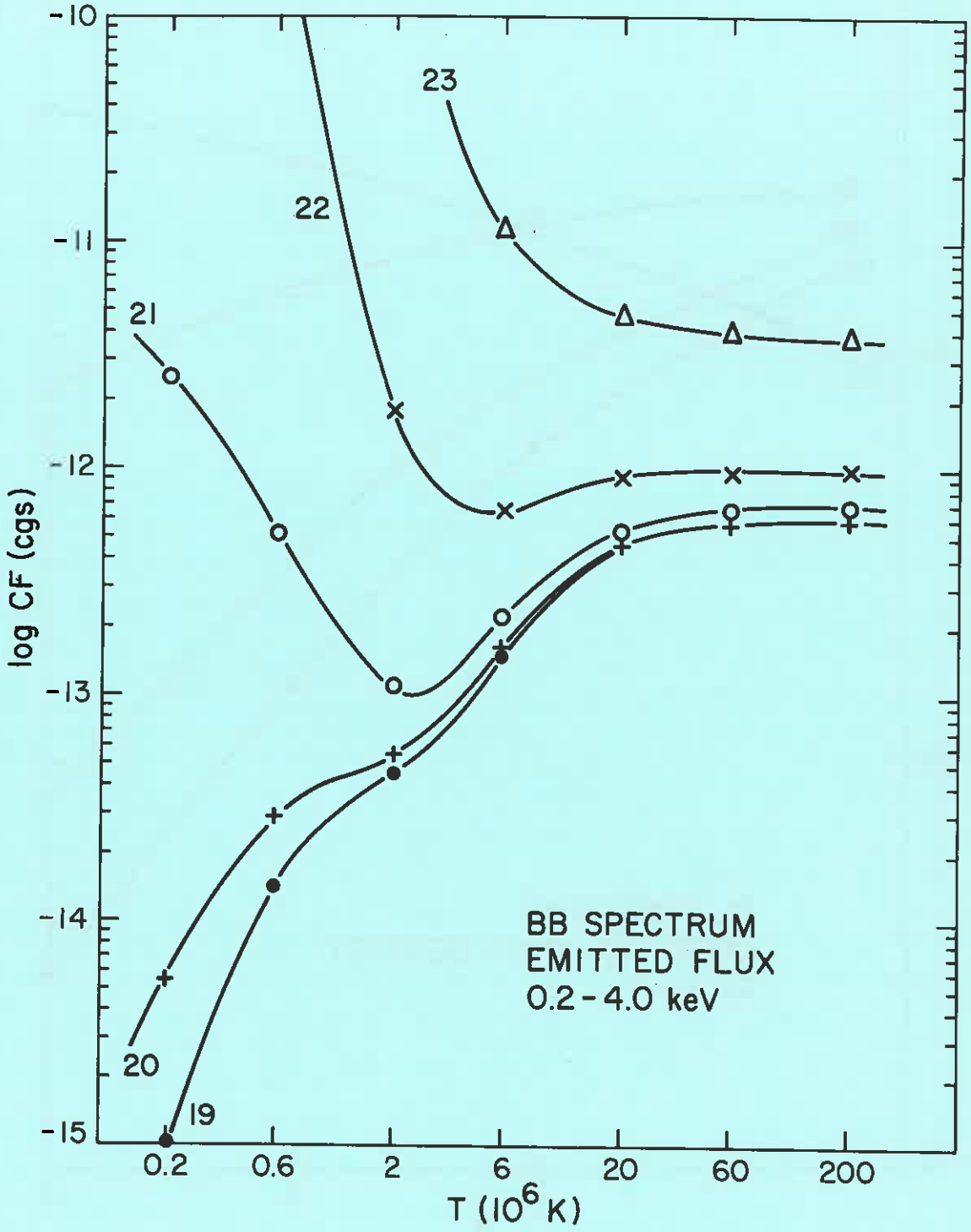

Figure 4.10.4D

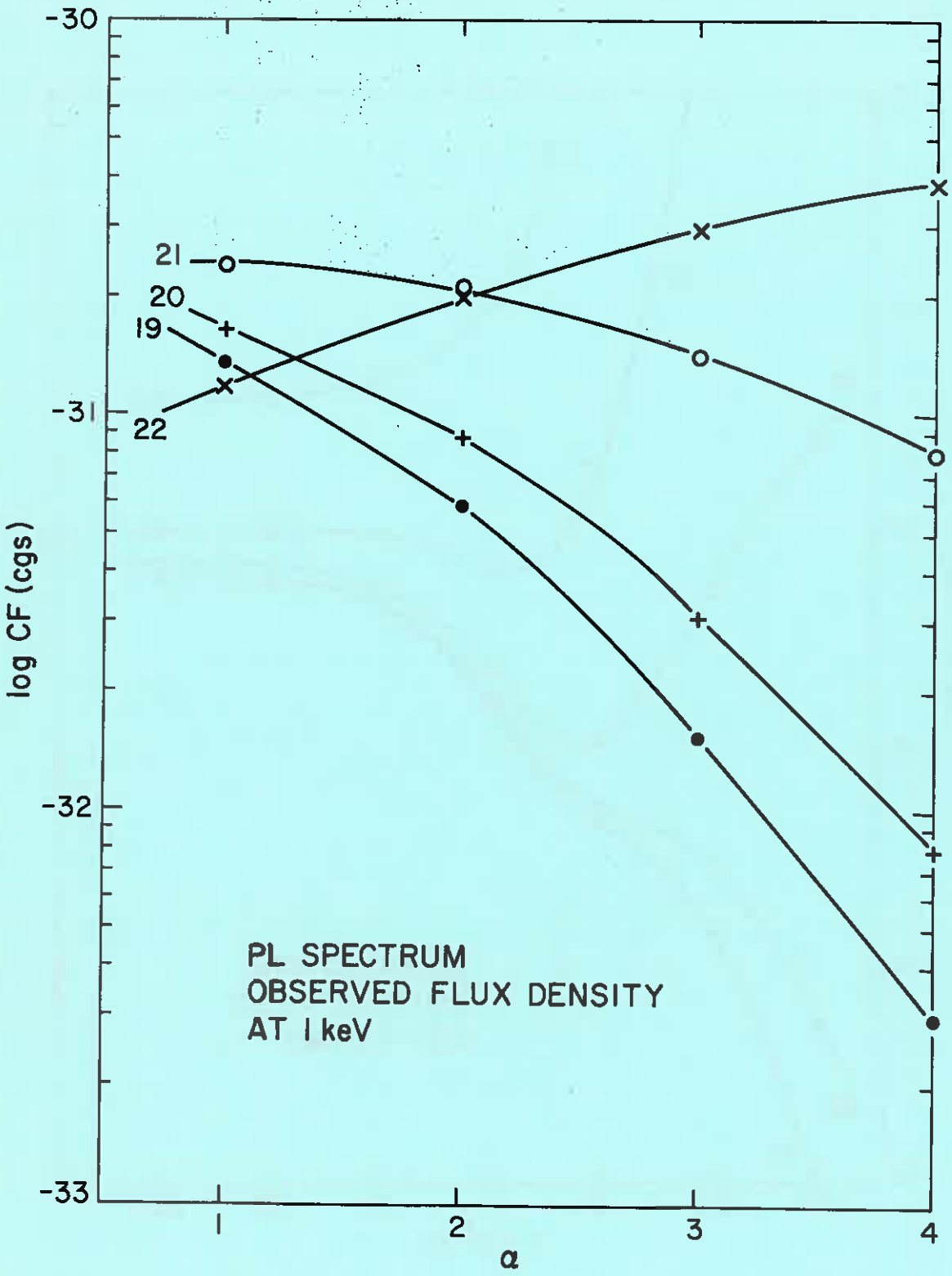

Figure 4.10.5A

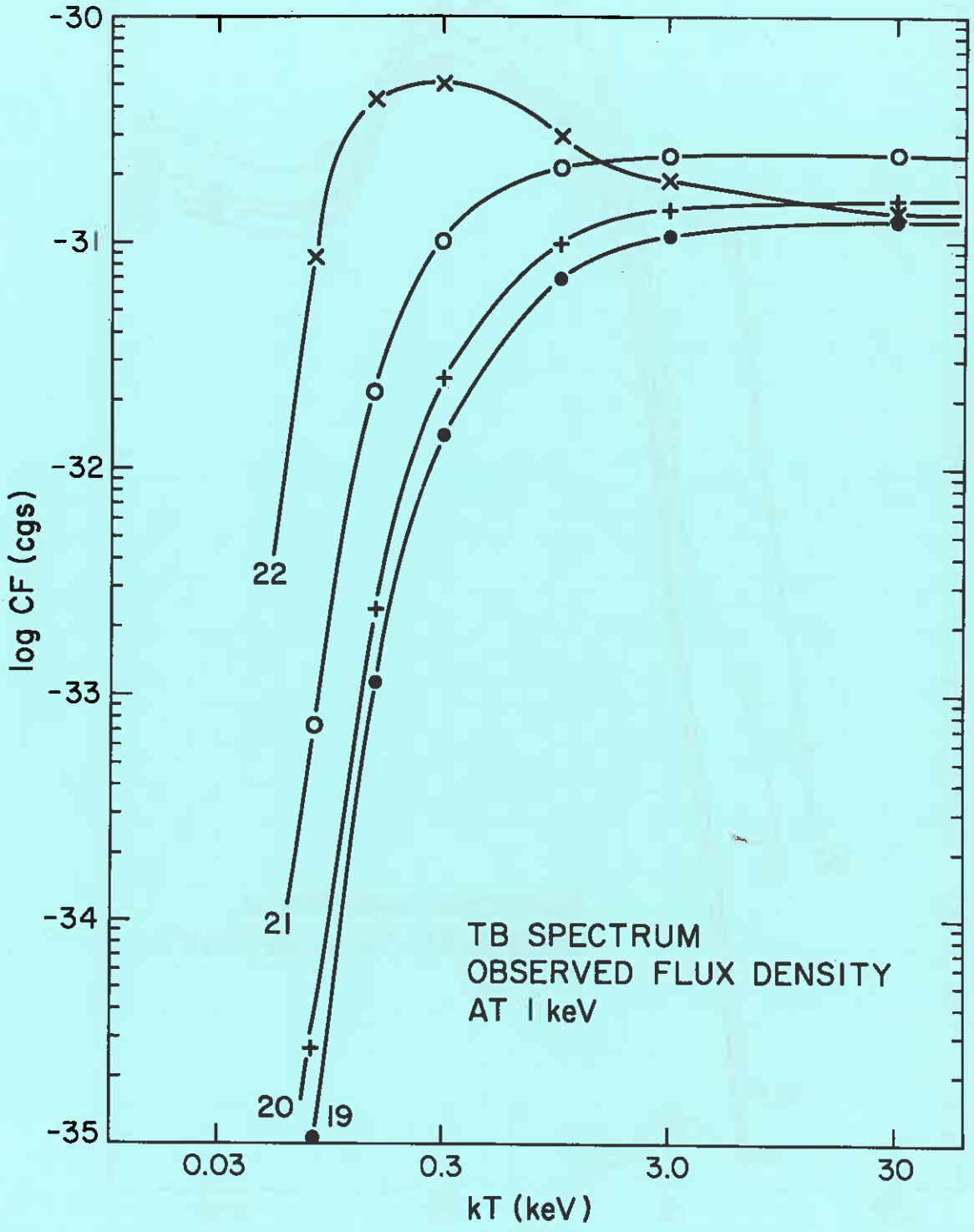

Figure 4.10.5B

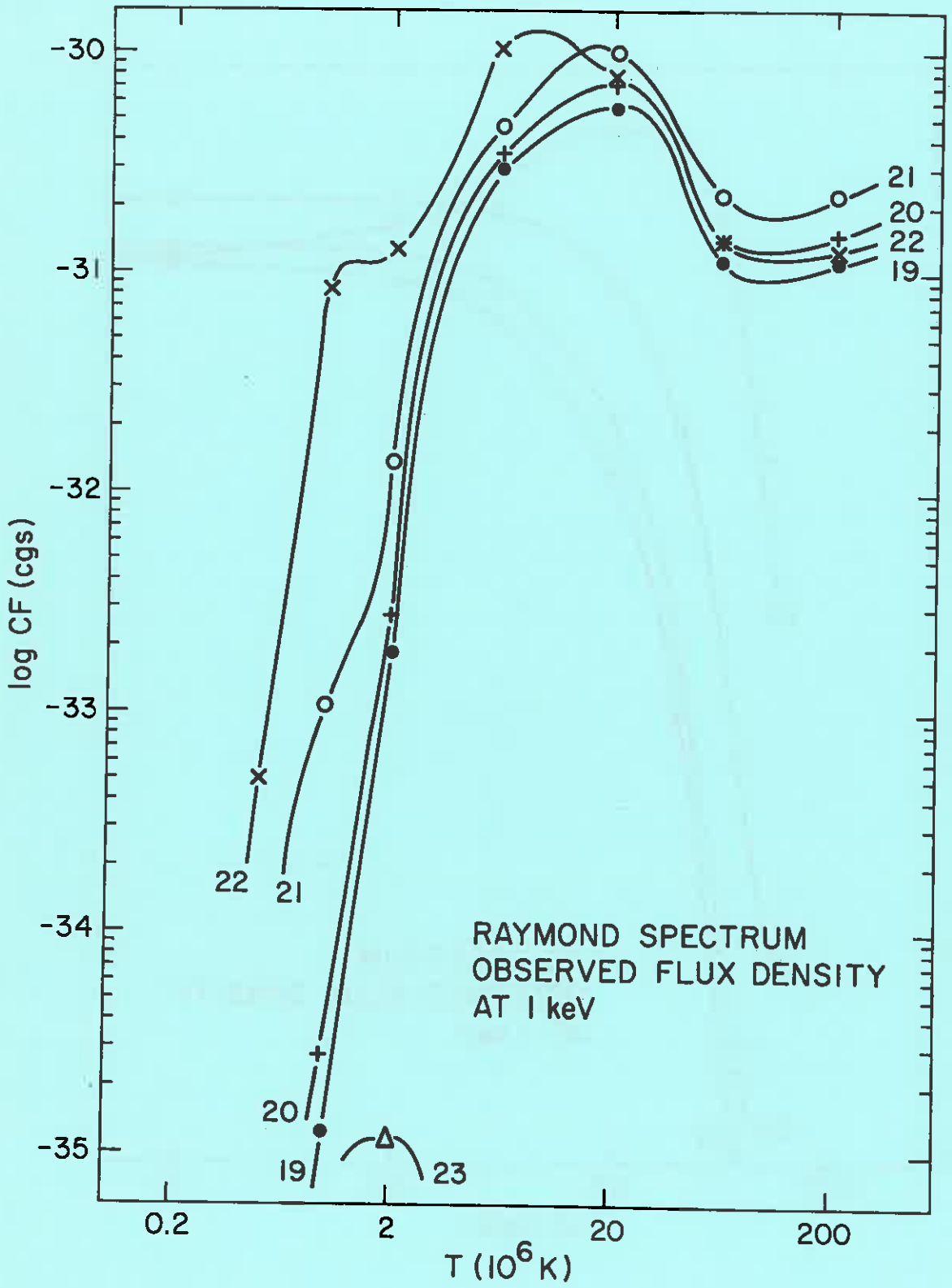

Figure 4.10.5C

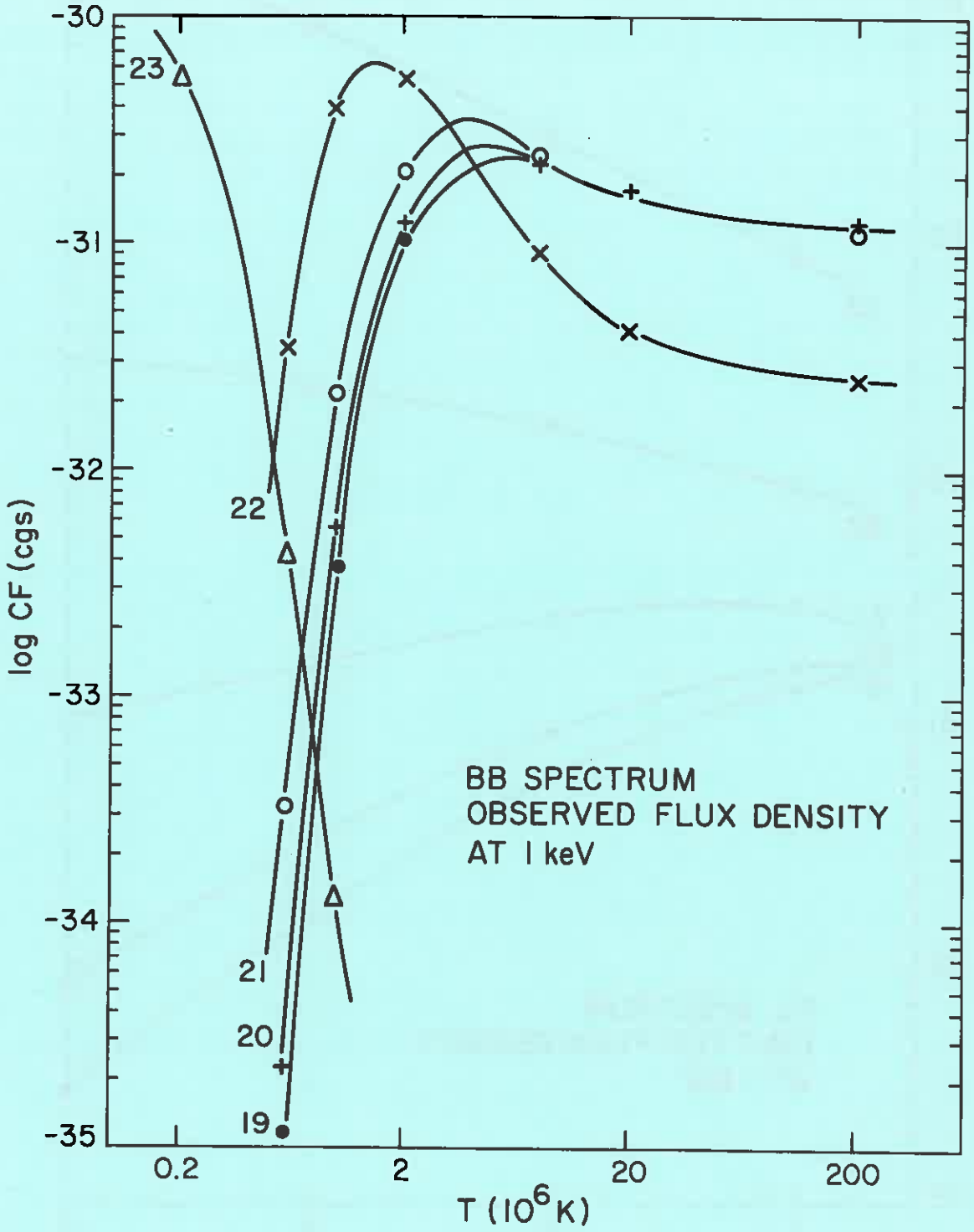

Figure 4.10.5D

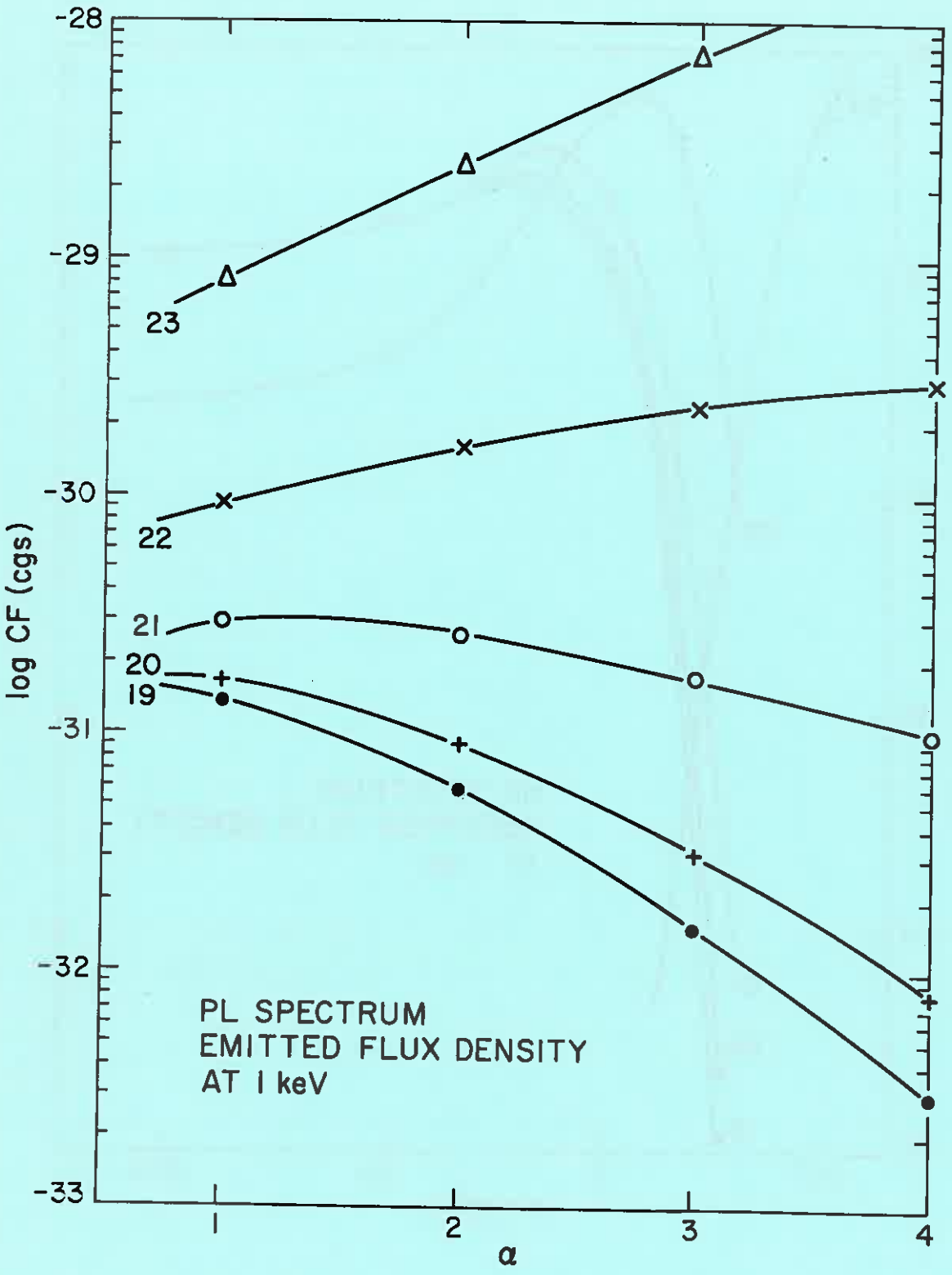

Figure 4.10.6A

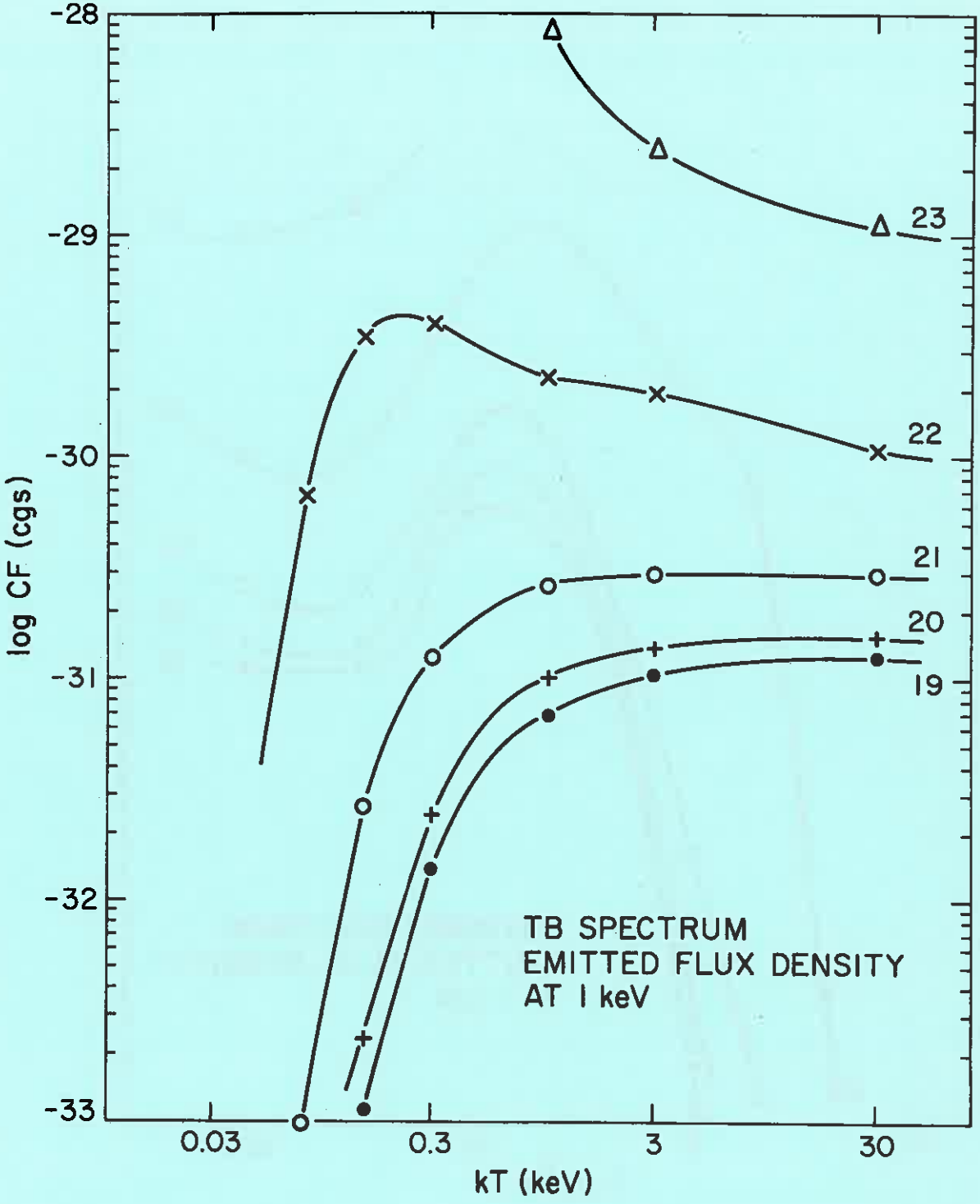

Figure 4.10.6B

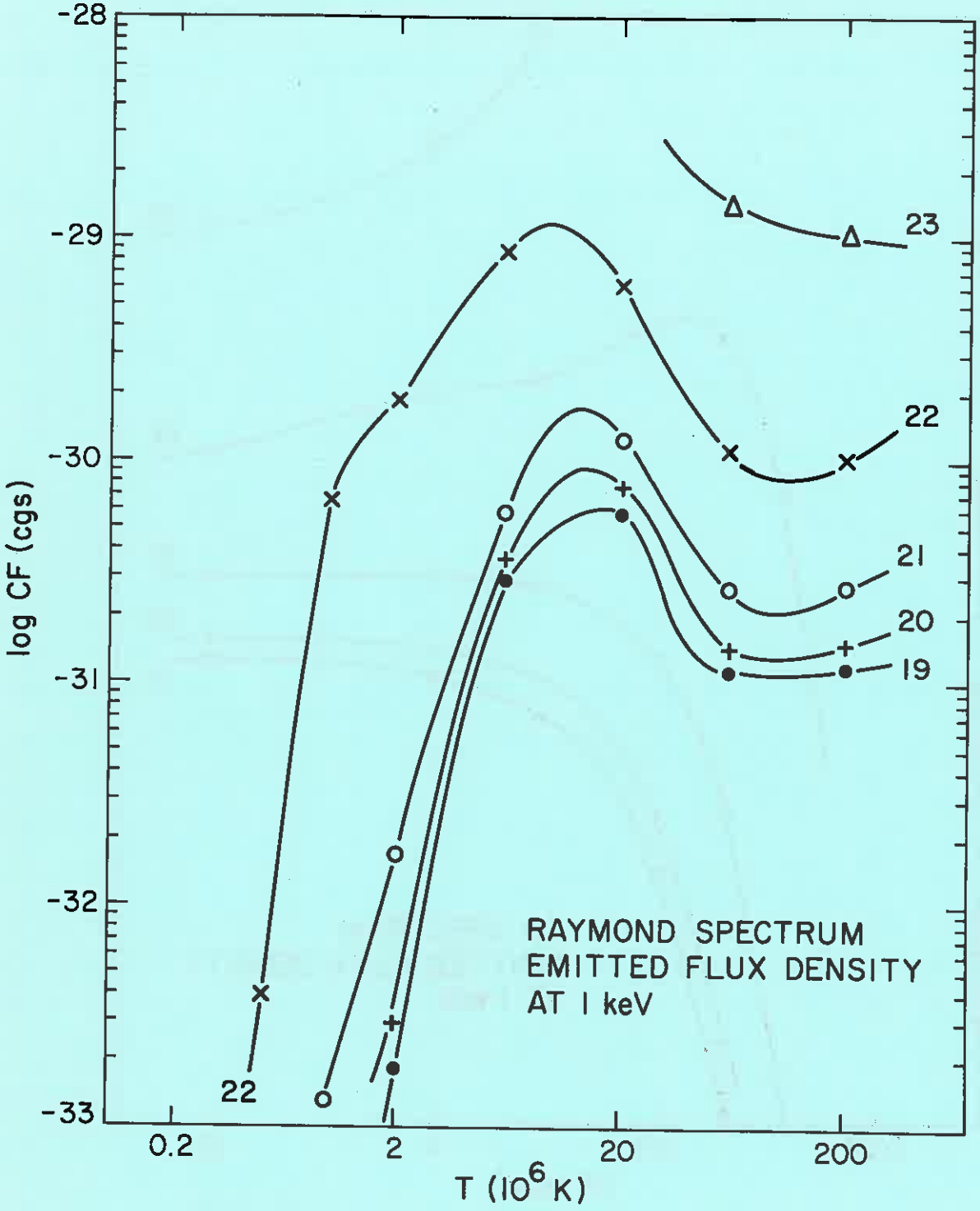

Figure 4.10.6C

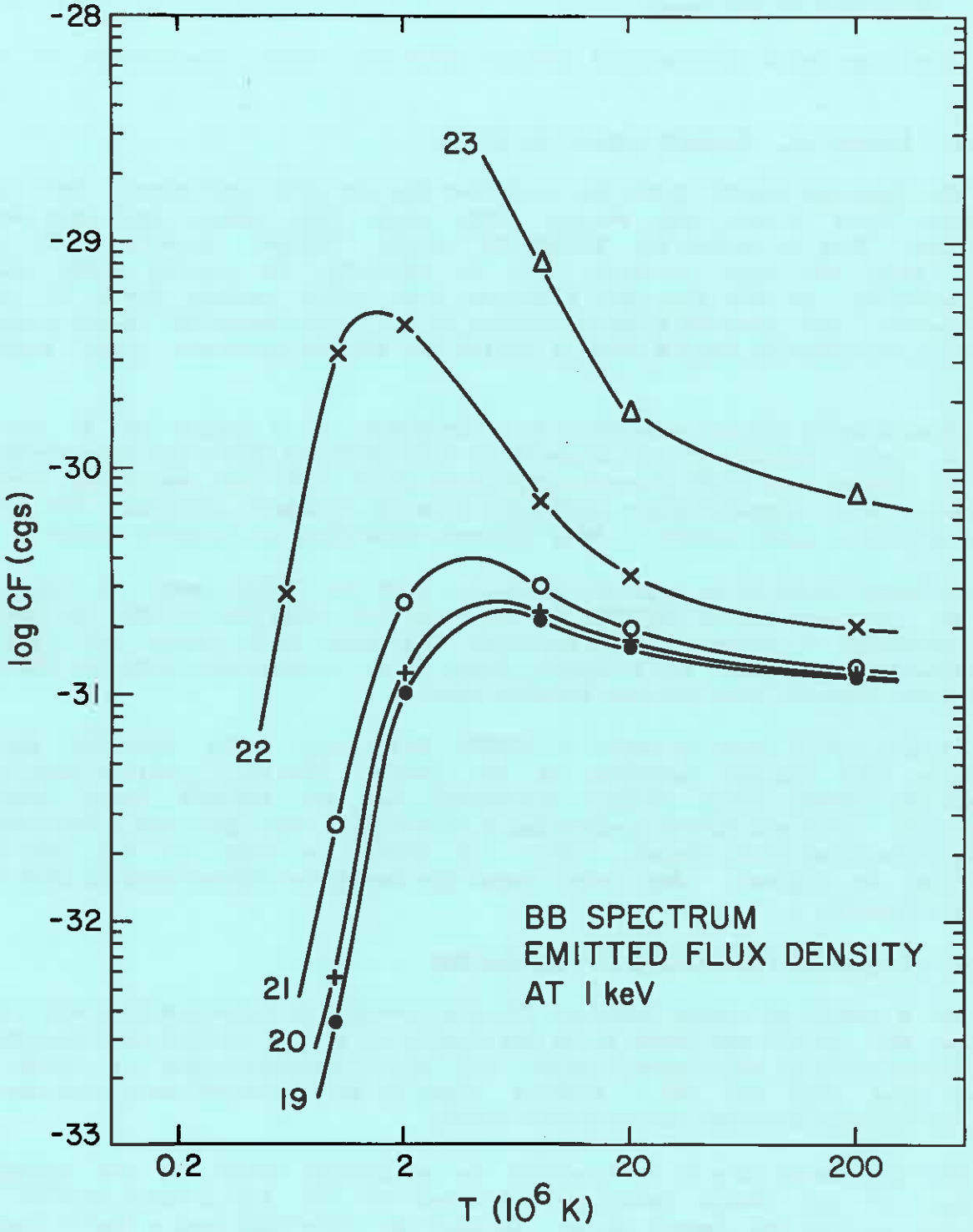

Figure 4.10.6D

4.11 Integrity of the Image

There are three instrumental effects which may cause distortions of the PRF.

4.11.1 Locked vs. Mapmode Aspect Solutions

The Einstein aspect (pointing) solution has two different modes. The star trackers first locate the chosen guide stars and report back only their positions. This is called the 'LOCKED-ON' or the 'LOCKED' solution. In the other mode the star trackers fail to identify the chosen guide stars unambiguously. In this case the trackers scan their entire field of view continuously and send back the positions of all stars detected. Since a piece of sky is continually mapped this is called the MAPMODE solution. (See section 3.4).

Occasionally sources are found to be extended on a scale of 4" to 8" because some segments of the observation were obtained while the star trackers were not locked onto their pre-assigned guide stars AND the resulting aspect solutions were significantly different from the "locked" solution. The total image of even a point source is thus blurred, mimicking an extended source.

Although there is no a priori guarantee that the LOCKED image is superior to that obtained during MAPMODE, in all cases (~6) examined at CfA, the LOCKED data produced a better X-ray position (agreeing with radio and optical counterparts) as well as a sharper image (i.e. consistency with the PRF for unresolved sources) than did the MAPMODE data.

Figure 4.11.1 shows an image of LOCKED data only. The circular cursor indicates the optical position of the galaxy. The Y, Z profiles show cuts through the LOCKED image (lower intensity) and the MAPMODE image (higher intensity). For all images containing a source with more than 100 total counts we have generated these images. They are stored on tape at CfA and are available on request. Any other image can easily be reprocessed to give the separate images.

4.11.2 Imperfect Corrections of the Gap Map

For a number of strong sources, the distribution of counts within the core of the PRF ($r<3"$) was found to be distinctly elliptical rather than circular. This effect must be instrumental since its major manifestation is found on scales less than the PRF. However, since it has "annoyed" more than one EO user, we briefly describe its probable cause.

The assignment of a Y, Z location to a photon rests on the relative response of the charge detectors attached to the wires which collect the electrons exiting the channel plate. Because the algorithm uses a finite number of adjacent wires (here 3) there will be gaps in each coordinate wherein it is electrically impossible to assign a photon.

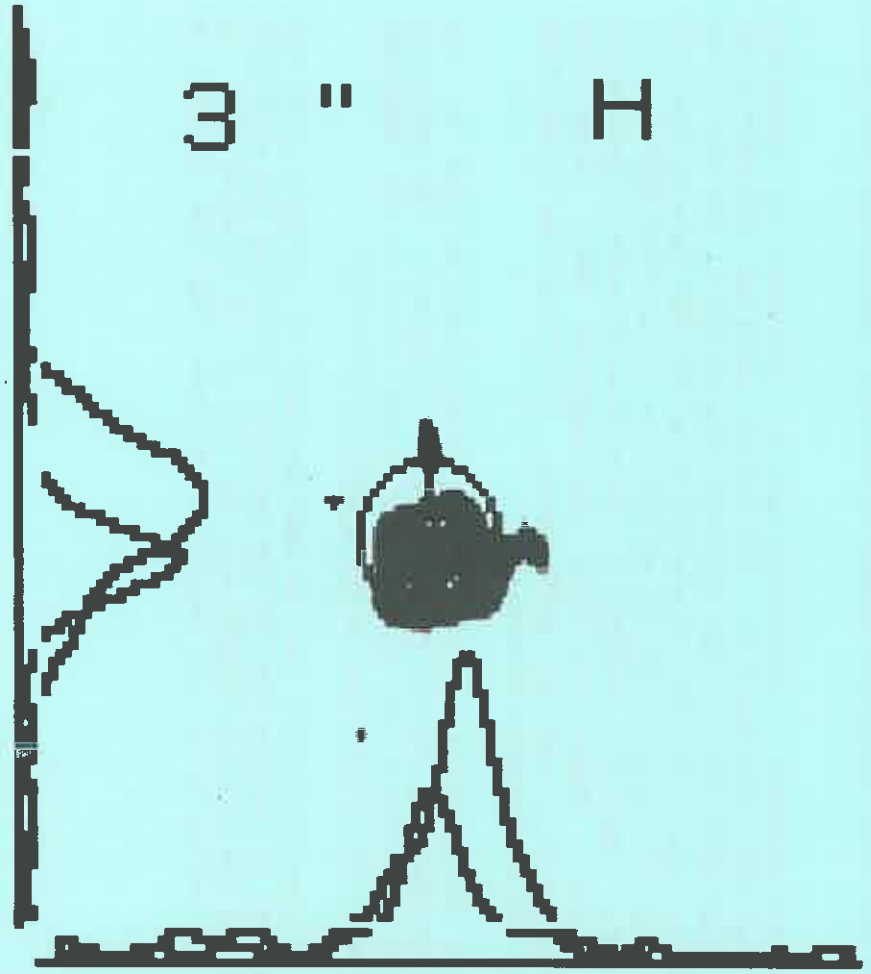

Figure 4.11.1

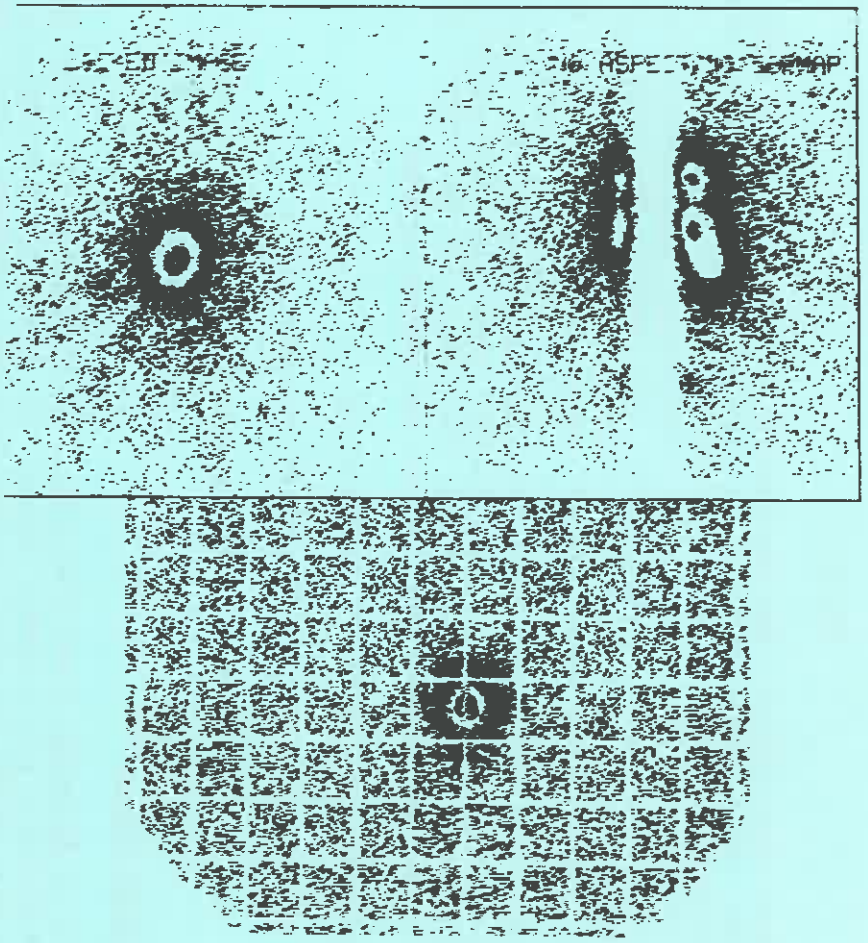

Figure 4.11.2

Figure 4.11.2 shows this effect. The gap structure is delineated by making a map without aspect corrections and without gap-map corrections, i.e. the image mapped in "detector" or "electrical" coordinates. At the upper left is the LOCKED image (see previous section) to the same scale. This results from the normal aspect corrections and corrections for the gaps. The GAPS are removed in the processing using a mapping (the GAPMAP) from electrical to detector co-ordinates. This GAPMAP was derived from observations of a UV calibration pattern and of a bright diffuse source (the Crab Nebula). However, because these corrections are imperfect, it is believed that they are the cause of the final elliptical distribution. For the example shown, the roll angle is 115°. Whilst this problem is usually noticed in the core of the PRF, the ramifications in the wings may be detectable for the strongest sources.

In detector coordinates gap locations are given by

$$gap(n) = 566.672 + (n - 1)\ 197.510 \text{ pixels}$$

i.e. 1.64 arcmin separation

4.11.3 "Confused" Guide Stars

The star trackers on Einstein found star positions by taking the centroid of light coming from within a box 2 arcmin square. In some cases a bright star near the chosen guide star moved the centroid away from the expected position. Diffuse nebulosity around the guide star had a similar effect. When this occurs, data segments may have incorrect ASPECT solutions, producing distorted images.

The presence of this problem is relatively easy to discover by examining the "Processed Data Log" (See section 4.2). The column labelled "SEP ERR" gives the difference (in arcseconds) between the observed separation of the two guide stars in the trackers and the true separation from the SAO catalog for each segment of the data. For the great majority of the data these "SEP ERR"s are in the range 0-6 arcseconds, sometimes reaching 8. Occasionally much larger values are found (10 to 20 arcsec). Whenever we have investigated these large "SEP ERR"s we have found cases of 'confused' guide stars. In one of the worst cases the guide star was in the 30 Doradus nebula.

If you have large "SEP ERR"s sections of data you may want to look at the guide stars on the Palomar Sky Survey to check for 'confusion'. The positions and SAO numbers of the guide stars for an observation are given in the 'APS.PRN' files which are available on microfiche in the Einstein data room.

It is possible to reprocess your data to exclude sections of data with bad "SEP ERR"s. This is done by running RESORT and manually selecting the good data intervals. Instructions for running RESORT may be found in Chapter 8. An automatic version of resort to select intervals of given 'SEP ERR' is part of our future plan.